AD A161 520 FATIGUE LIVES OF SPECIMENS REPRESENTING CRITICAL LOCATIONS IN MIRAGE III S..(U) AERONAUTICAL RESEARCH LABS MELBOURNE (AUSTRALIA) J Y MANN ET AL. FEB 85 1/1

UNCLASSIFIED ARL/STRUC-R-415 F/G 1/3 NL

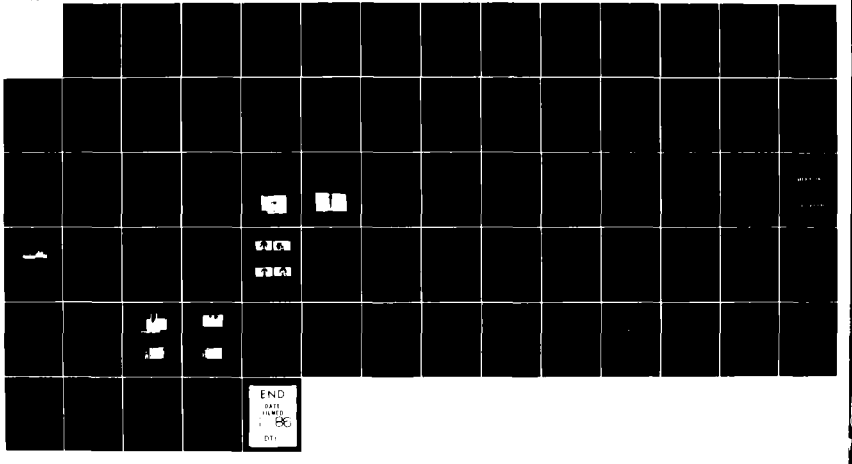

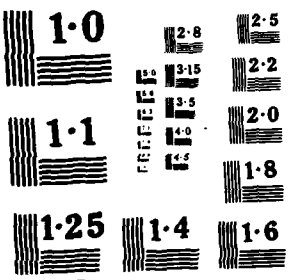
1·0
1·1
1·25
1·4
1·6
2·8
3·15
3·5
4·0
2·5
2·2
2·0
1·8

ARL-STRUC-R-415

(12)

AR-003-998

AD-A161 520

DEPARTMENT OF DEFENCE

DEFENCE SCIENCE AND TECHNOLOGY ORGANISATION

AERONAUTICAL RESEARCH LABORATORIES

MELBOURNE, VICTORIA

STRUCTURES REPORT 415

FATIGUE LIVES OF SPECIMENS REPRESENTING CRITICAL LOCATIONS IN MIRAGE III SPARS UNDER AUSTRALIAN AND SWISS TEST SPECTRA

by

J. Y. MANN and G. W. REVILL

DTIC
ELECTE
NOV 26 1985
S D

THE UNITED STATES NATIONAL TECHNICAL INFORMATION SERVICE IS AUTHORISED TO REPRODUCE AND SELL THIS REPORT

DTIC FILE COPY

Approved for Public Release

© COMMONWEALTH OF AUSTRALIA 1985

COPY No

FEBRUARY 1985

11 21 85 038

AR-003-998

DEPARTMENT OF DEFENCE
DEFENCE SCIENCE AND TECHNOLOGY ORGANISATION
AERONAUTICAL RESEARCH LABORATORIES

STRUCTURES REPORT 415

FATIGUE LIVES OF SPECIMENS REPRESENTING CRITICAL LOCATIONS IN MIRAGE III SPARS UNDER AUSTRALIAN AND SWISS TEST SPECTRA

by

J. Y. MANN and G. W. REVILL

SUMMARY

Full-scale flight-by-flight fatigue tests on Mirage III fighter aircraft wings carried out at the Australian Aeronautical Research Laboratories (ARL) and the Swiss Eidgenössisches Flugzeugwerk (F+W) indicated much greater differences in the flights to failure than were expected. This problem has been investigated by conducting fatigue tests on specimens representing the major failure locations in the test wings — a blind anchor-nut hole in the Australian case and an interference-fit bolt hole in the Swiss case — under flight-by-flight loading sequences corresponding to those used in the full-scale tests. Constant-amplitude fatigue tests were also carried out on the blind-hole specimens to provide information for life estimation purposes, and fractographic crack propagation studies were conducted on selected blind-hole specimens.

The experimentally determined lives of both types of specimen were greater under the Australian than the Swiss stress spectrum. Depending on the stress scaling factor considered the life ratio (Australian/Swiss flights) obtained by grouping together the two stress spectra and the two types of specimens were between about 3 and 4·2. This compares with a ratio of 4·6 obtained for the respective full-scale wing fatigue tests.

For the blind anchor-nut hole specimens the predicted fatigue lives were less than those obtained experimentally at high stress scaling factors, but at low stress scaling factors the converse was the case. The ratios of the predicted lives to failure (Australian/Swiss) were much greater than those found experimentally.

Under both the Australian and Swiss stress spectra, the lives of front-flange bolt hole specimens incorporating interference-fit bolts were between 3 and 4 times greater than those with clearance-fit bolts.

© COMMONWEALTH OF AUSTRALIA 1985

POSTAL ADDRESS: Director, Aeronautical Research Laboratories,
Box 4331, P.O., Melbourne, Victoria, 3001, Australia

CONTENTS

Accesion For
NTIS CRA&I ☑
DTIC TAB ☐
Unannounced ☐
Justification .....
By .....
Distribution /
Availability Codes
Dist | Avail and / or Special
A-1

QUALITY INSPECTED 3

1. INTRODUCTION

During 1974 the Aeronautical Research Laboratories (ARL) carried out a full-scale flight-by-flight fatigue test on the starboard wing of a Mirage IIIO aircraft under a loading spectrum based on the then current usage of the aircraft by the Royal Australian Air Force (RAAF). In this test the wing was mounted on a dummy fuselage which was designed to produce the correct flexibilities and reactions at the attachment points. It terminated with the catastrophic failure of the main spar after a life of 32,372 simulated flights. Details of the test and of the failures which occurred in the wing are given in References 1 to 3.

Although considerable fatigue cracking was found at different locations in the structure, the failure which led to its eventual collapse originated at a small drilling "dimple" at the bottom of a blind hole in the lower (tension) spar cap. A press-fitted and adhesively-bonded anchor nut had been inserted in this hole to form part of the wing fixed fairing attachment system. Figure 1 shows the general location of the failure in the wing spar, while Figure 2(*a*) details the particular section. The extent of the fatigue cracking in relation to the fastener hole is shown in Figure 2(*b*). This clearly indicates the dimple at the bottom of the hole where the crack initiated. The results of a fractographic analysis of the spar fracture surface are contained in Reference 4, and the significance on the fatigue life of a "dimpled hole" compared with a hole having a true spherical bottom has been discussed in Reference 5.

Subsequent to the ARL test a full-scale fatigue test on a complete Mirage IIIS structure was carried out by the Eidgenössisches Flugzeugwerk (F + W), Emmen, Switzerland using a spectrum based on Swiss Air Force (SAF) Mirage operations. The test terminated at 7,248 flights when a catastrophic failure of the port wing occurred from a crack which had initiated at a 5 mm diameter bolt hole (hole no. 12) on the forward flange (Figures 1 and 3). The particular bolt was part of the system for attaching the skin of the wheel well to the spar flange and was nominally an interference-fit fastener. Details of this fracture in the Swiss port wing are given in Reference 6.

Although the Swiss fatigue test on the Mirage was carried out under a generally more severe loading spectrum than the ARL test, the difference in lives to failure were much greater (by a factor of 3) than predicted on the basis of a simple comparison of stresses in the failure regions under the two test spectra. An important implication of this analysis was that, unless this difference in lives could be satisfactorily explained, previous estimates of the safe-life of the Mirage wing structure might have been unconservative. As a consequence ARL undertook several theoretical and experimental studies (Refs 7-9) in an attempt to resolve the problem. The present report covers an experimental investigation to compare the fatigue lives of specimens representing the two major failure locations in the Mirage wing main spar during the ARL and F + W full-scale tests, when tested under both the Australian and Swiss load spectra.

2. FATIGUE TEST SPECTRA

Figure 4 indicates the load spectra used for the ARL (Reference 10) and F + W (Reference 11) full-scale Mirage structural fatigue tests.

The development of the test loading spectrum/sequence for the ARL wing test is summarised in References 1 and 2 and fully described in Reference 10. It was derived from the averaged fatigue meter data obtained during RAAF squadron usage of the Mirage IIIO in the 1971-72 period, and extensive flight trials using specially instrumented aircraft to determine strains and strain-time sequences under particular types of operational missions. A 500-flight flight-by-flight sequence was adopted (each flight representing an average of about one service hour) which provided the correct mix of the variety of mission types experienced by the aircraft in service.

It consisted of 55 mission types, 137 load cases, seven pilot skill/aircraft handling multiplying factors and optional gust loading, and resulted in the selection of about 400 different types of flight. Some flights were repeated to provide the balance up to 500. Each flight included between 35 and 629 individual load excursions and, within each flight, the load sequence was designed to be representative of the sequence of occurrence of manoeuvre loads, gust loads, ground loads and fuel tank pressurization loads. The ARL wing fatigue test was controlled and monitored through a PDP-11 computer, the control magnetic tape providing one application of the maximum positive load of the sequence (+7·8 g) during Flight 65, and six applications of the greatest negative load (−1·0 g) during each 500-flight sequence. In addition, (during the full-scale wing test only) a single "rarely occurring" high positive load (of +8·5 g) was applied manually at about 5000-flight intervals.*

The Swiss test load spectrum was derived from fatigue meter records taken between 1972 and 1974 from the average of the six most severely loaded aircraft in the Swiss Mirage fleet, supplemented by strain data obtained from the test flying of a more fully instrumented aircraft (Reference 11). Typical missions were defined and identified by 24 "typical" flights (each representing an average duration in service of about 40 minutes) which were then combined in their correct statistical distribution to provide a test sequence containing 200 flights. Table 1 (Reference 6) gives the order of occurrence of the 24 distinct flights in the 200-flight sequence. Each typical flight consisted of three of four segments (representing, for example, take off, combat, landing), the actual load sequence in each being appropriate to the particular segment. The maximum load of the sequence (+7·5 g) occurred twice in each sequence of 200 flights — in flights 48 and 150. In the Swiss test the negative side of the spectrum was much more severe than in the ARL test, with the greatest negative load (−2·5 g) being applied twice in every 200-flight block. Further details relating to the Swiss test may be found in References 9 and 12.

3. TEST SPECIMENS AND MATERIALS

The main spar of the Mirage III is a large forging in aluminium alloy to the French Specification A-U4SG (equivalent to the American alloy 2014 which is covered by Specification QQ-A-255a). As inadequate quantities of A-U4SG were available at the time, the test specimens used in this investigation were made from two similar (but not identical) British alloys, namely B.S. 2L65 and B.S. L168 supplied originally in the form of extruded bars.

3.1 Blind anchor-nut hole specimens

The type of specimen adopted is shown in Figure 5. It incorporated a feature which represented the blind anchor-nut fastener hole in the spar at which the ARL test wing failed and three different types of detail.

(i) Type 'A'— a hole with a spherical bottom (as specified on the spar manufacturing drawing).
(ii) Type 'B'— a spherical-bottom hole with a superposed drill point or "dimple" (similar to the actual anchor-nut holes in Australian wings).
(iii) Type 'C'— Types 'A' or 'B' but with a threaded-hole interference-fitted steel bush representing the anchor nut. The bush was not adhesively-bonded into the hole, in case surplus adhesive at the bottom of the hole masked the observation of cracks.

All of the blind-hole specimens were manufactured from the grip portions of broken fatigue specimens of 2L65 aluminium alloy tested in a previous investigation (Reference 13), which

* Because of its association with particular loading cases this load produced strains in the spar which were less than those resulting from the applications of the more frequent +7·8 g load.

involved two batches of extruded material designated BJ and CL. The general plan form of the original specimens, together with the locations from which the smaller specimens were taken, is shown in Figure 6. The relevant Specification requirements for A-U4SG and 2L65 are given in Table 2, together with the tensile and fracture toughness properties of the BJ batch of 2L65 material which was used for this part of the investigation.

3.2 Front flange specimens

The front flange specimens (Figure 7) represented the detail at the 12th to 16th bolt holes along the front flange of the spar, the thickness of the test section (28 mm) corresponding to the nominal thickness of the flange at the 12th bolt hole. These specimens were machined from 63·5 mm × 31·75 mm extruded bars of B.S. L168 aluminium alloy (laboratory code GR) with their longitudinal axes parallel to the direction of extrusion. They were identical to the general type of specimen used for a previous ARL investigation relating to the refurbishment of the Mirage spar (Reference 14), but for the current investigation the specimens incorporated only clearance-fit or interference-fit 5 mm diameter bolts. In the latter the bolt holes were reamed to very close tolerances to accept bolts with nominally 0·4% to 0·8% interference. However, because of practical difficulties associated with compressive bulging of the bolts during installation which prevented those providing the higher interference from being fully inserted in the holes, the maximum value was maintained at about 0·4% by careful hole sizing and selection of bolts of the appropriate diameter.*

Tensile test specimens were taken from broken fatigue specimens. Compact tension fracture toughness specimens (thickness 25 mm and 19 mm) were taken from offcuts of the extrusion at the positions shown in Figure 8. Specification values covering the tensile properties and chemical composition for the alloys A-U4SG and L168 together with those derived from tests on the particular batch of material used and the fracture toughness values, are also given in Table 2.

4. FATIGUE TESTING PROGRAM

During the Australian full-scale Mirage wing test the strains at various positions in the structure were recorded at every load turning point, and the load sequence which was applied to both the blind hole and front flange specimens was derived from the strains recorded at a strain gauge (position 1·4T which was located near hole no. 12) during one 500-flight block. Similarly, for tests under the Swiss sequence, the strain sequence corresponded to that at hole no. 12 in the Swiss full-scale wing test. The actual strains were determined during the strain survey detailed in Appendix I.

All fatigue tests were carried out in axial loading using a 600 kN capacity MTS electro-hydraulic fatigue testing system, under computer control and with the Australian and Swiss test strain sequences stored on magnetic tapes. The resulting load sequences experienced by the specimens were of quasi-sinusoidal wave form.

4.1 Derivation of test stress levels

For both the blind hole specimens and the front flange specimens the test stresses were selected (in the first instance) to nominally correspond to those which occurred at the features which they represented in the respective full-scale wing tests. In the case of the blind hole specimens the nett area was used to calculate the applied loads. Although the test loads for the front

* The specific bolt hole identification system, (1) to (5), adopted in this investigation is indicated on Figure 7.

flange specimens were calculated using the gross area, they were such as to give the same nett-area stresses in an interference-fit bolt specimen as those which occurred in the respective full-scale wing tests. This procedure was considered to provide a better comparison for specimens of different nett area, i.e. with clearance-fit rather than interference-fit bolts.

Tests were also carried out on both types of specimen and under each of the two sequences in which the stresses were increased by various 'scaling factors' to cover a situation where the actual stress in the spar may have been greater than the reference stress originally assumed. The "scaling factor" was defined as in Figure 9, the reference stresses derived from the full-scale tests being regarded as corresponding to scaling factors of unity.

As the chordwise locations in the spar of neither the blind hole nor the bolt hole no. 12 corresponded exactly to that of strain gauge 1·4T, multiplying factors were developed to determine the stresses at these two positions of interest. The stresses were:

At the blind hole, 1·14 × stress indicated at gauge 1·4T.

At hole no. 12, 1·20 × stress indicated at gauge 1·4T.

Under the Australian sequence the specimen stresses corresponding to the maximum positive peak load of the sequence (+7·8 g) at a scaling factor of unity were:

Blind hole:	Nett-area stress 155 MPa
	Gross-area stress 133 MPa
No. 12 bolt hole:	Nett-area stress 163 MPa
	Gross-area stress 146 MPa

A small offset was accidently introduced into the Australian sequence applied to these specimens. This had its maximum effect at the greatest negative turning point when the magnitude of the stress was reduced by approximately 20%. The offset was zero at the greatest positive turning point, and was proportional in between these limits.

Under the Swiss sequence the maximum stresses (corresponding to +7·5 g) for each type of specimen at a scaling factor of unity were:

Blind hole:	Nett-area stress 223 MPa
	Gross-area stress 191 MPa
Bolt hole no. 12:	Nett-area stress 235 MPa
	Gross-area stress 211 MPa

It should be noted that, for the Swiss sequence, stress and "g" were linearly related. Because of different loading cases within individual flights (associated, for example, with fuel usage, elevon operation, the use of air brakes) there was not a unique stress/g relationship for every value of "g". On the other hand, for the Australian sequence, the stress/g relationship was bi-linear (Reference 9) and, depending on the particular flight parameters being represented (e.g. altitude or airspeed, stores configuration, fuel usage) the stresses at the higher values of "g" – exceeding 4 g to 5 g – were considerably less than would be predicted by a linear stress/g relationship at lower values of "g" (References 10 and 12).

4.2 Blind anchor-nut hole specimens

This investigation included a total of 27 constant-amplitude fatigue tests under sine-wave loading on bushed and non-bushed hole specimens of the two Types "A" and "B" at a mean stress on nett area of 47·8 MPa (gross-area stress 41·4 MPa) and cyclic frequency of 6 Hz, the object of which was to provide more specific background fatigue data on this type of detail

for *life-estimation purposes*. A total of 36 tests was carried out on bushed-hole specimens (of Types "A" and "B"), 21 under the Australian Mirage flight-by-flight loading sequence and 15 under the Swiss flight-by-flight sequence to compare the two loading sequences.

Figure 10 indicates the cumulative frequency stress spectra for both the Swiss and Australian sequences at a scaling factor of unity. Figures 4 and 10 clearly illustrate the differences between the cumulative frequency stress spectra and load spectra for the two sequences, in particular the significance of the bi-linear stress/g relationship in the Australian case at "g" values exceeding about 4. Figure 10 also shows that the Australian sequence incorporates a much greater number of low-amplitude stresses than does the Swiss.

Stress scaling factors of up to 2·6 were used with the Australian sequence, and to 2·2 for the Swiss sequence. The stresses corresponding to the maximum "g" loads at different scaling factors are given in Table 3. It should be noted that for a scaling factor of 2·2 in the Swiss sequence the nominal nett-area stress at +7·5 g is 490 MPa, which is only about 5% less than the ultimate static strength of the 2L65 test material.

The computer programs used for these tests generated a load command signal for which the time between turning points depended upon the amplitude of the excursion. Most of the tests under the Australian sequence were carried out with effective frequencies of *individual load* excursions that varied from about 1·4 to 18 Hz, with an average over 500 flights of 4·6 Hz. At this average cyclic frequency, a 500-flight block (which consisted of about 50,000 cycles) took about three hours to complete. Some of the early tests under the Australian sequence were, however, carried out (as noted in Table 5) at average cyclic frequencies of either 1·1 or 1·3 Hz. All of the tests under the Swiss sequence were at an average frequency of 9·3 Hz, and a 200-flight block (of about 20,000 cycles) took about 36 minutes to complete.

4.3 Front flange specimens

A total of 27 specimens of this type were fatigue tested. They included 14 under the Australian sequence (six interference-fit bolts and eight clearance-fit bolts), and 13 under the Swiss sequence (six interference-fit bolts and seven clearance-fit bolts).

Fatigue tests were carried out using stress scaling factors of from 1·12 to 1·67 for the Swiss sequence, and 1·34 to 2·23 for the Australian sequence. For the maximum scaling factors the respective nett-area stresses at the maximum "g" values were 393 MPa and 364 MPa.

Fatigue tests under the Swiss sequence were carried out at an average cyclic frequency of 9·3 Hz, while those under the Australian sequence were at 4·6 Hz. A trace of the stress sequence under the Swiss spectrum around flights 48 and 150 is shown in Figure 11, while that for the Australian sequence around flight 65 is shown in Figure 12.

5. TEST RESULTS

5.1 Blind anchor-nut hole specimens

5.1.1 Constant-amplitude tests

The results of the constant-amplitude fatigue tests on the three different types of detail are listed in Table 4 and shown in Figures 13 and 14. A second order polynomial was found to provide the best-fit S/N curve for the bushed dimpled specimen data shown in Figure 14. In only two cases (indicated by asterisks on Figure 13) did the fatigue crack originate at the bottom of the hole; both were dimpled non-bushed specimens and had lives of 7,644,000 (BJ18E2) and 9,425,500 cycles (BJ10F) respectively. In all other non-bushed specimens the cracks initiated at or close to the bottom edge of the chamfer at the top of the hole and propagated outwards and towards the bottom of the hole. This region was also a major initiation site in bushed-hole specimens but, in addition, cracks initiated as the result of fretting between the hole and the bush. Three exceptions were specimens in which the main origins were at the spherical surface of the hole, but not at the bottom.

The "run-out" specimen shown on Figure 14 was tested statically and failed at a nett-section stress of 527·5 MPa. This compares with an average UTS for this batch of material of 510 MPa. No fatigue cracks were detected on the fracture surfaces of this specimen.

5.1.2 Flight-by-flight tests

All of the tests under the Australian and Swiss flight-by-flight sequences are listed in Table 5 and plotted on Figure 15. With the exception of the three specimens tested at a scaling factor of 1·4 (BJ7F, BJ12D and BJ11JB) all of the failures in the dimpled hole specimens tested under the Australian sequence originated at the dimple and were generally similar in appearance to that which occurred in the ARL test wing - see for example Figure 16(*a*), specimen BJ13D. In the cases of specimens BJ7F and BJ11JB two major cracks developed, one from the dimple and the other from fretting adjacent to the bottom of the bush; whereas in specimen BJ12D the failure initiated solely from fretting adjacent to the bottom of the bush. For the spherical-bottom hole specimens a failure originating at the bottom of the hole occurred in only one case, namely specimen BJ18E1 tested at a stress scaling factor of 2·2, but nevertheless secondary cracks had developed from the bottom corner of the chamfer. The other fractures in spherical-bottom specimens were characterised (Figure 16(*b*) specimen BJ8H) by multiple crack initiation sites at the bottom corner of the chamfer, by fretting between the bush and the hole, and around the radius at the bottom of the hole.

Under the Swiss sequence the primary cracking in dimpled-hole specimens developed from the dimple in all but two cases – these being two very short life specimens (BJ10IB and BJ15JB) tested at a scaling factor of 2·2 where there were multiple initiation sites from the bottom of the chamfer, down the hole and at the dimple. However, in all specimens, there was some evidence of secondary crack initiation at these other sites - see for example Figure 16(*c*), specimen BJ6HB. Although only three spherical-bottom bushed specimens were tested under the Swiss sequence all indicated multiplicity of crack initiation at the various sites already referred to, e.g. specimen BJ12F Figure 16(*d*).

5.2 Front flange specimens

Individual fatigue test results for the front flange specimens tested under the Australian and Swiss sequences are given in Table 6 and shown on Figure 17. Specimen No. GR24A, which was unbroken after 102,656 flights of the Swiss sequence, was tested statically and failed through holes 4 and 5 at a nett-section stress of 476 MPa (gross-section stress 427 MPa). Small fatigue cracks were present at hole no. 4.

Three specimens (all of the interference-fit bolt type) failed in the grips. The fracture surfaces of all of the other front-flange specimens broken in the investigation are shown diagramatically in Figure 18, and photographs of representative fractures are illustrated in Figure 19. These show that holes no. 2 and no. 4 predominated as the holes from which the major fatigue crack development occurred, and that in only two specimens (both interference-fit bolt) of the 23 which failed in the test section did the cracks develop from other holes, i.e. no. 1 and no. 5. However, the actual fracture paths in eleven of the specimens (mainly those with clearance-fit bolts) passed through an adjacent bolt hole and about half of these provided evidence of fatigue cracking at these holes. With one exception (specimen GR25C – Swiss, clearance-fit) the fatigue cracking at the second hole was relatively minor. With the exception of five of the interference-fit bolt specimens, the primary fatigue crack development was from multiple initiation along the bore of the bolt hole, leading to a final crack shape approximating (in some cases) to a through crack. In the five interference-fit bolt specimens the crack development was concentrated at one end of the hole (in four cases at the nut end) leading to the development of a crack shape approximating to a double-corner crack. These cracking characteristics are similar to those reported previously (Reference 14) for the same types of specimens.

6. FATIGUE CRACK PROPAGATION

Fractographic crack propagation studies were made on a number of blind anchor-nut hole specimens which incorporated the drilling dimple and the steel bushes. These included two specimens (BJ9GB and BJ10JA) which had been tested under the Australian sequence and seven specimens under the Swiss sequence -- BJ7IB, BJ6HB, BJ7C, BJ4GB, BJ6JB, BJ4JB and BJ6C. The fractographic techniques employed included the use of macrophotographs, an optical stereo microscope and a metallurgical microscope at up to $\times 500$ (References 16 and 17). Incremental crack growth measurements were made in a direction backwards from the maximum boundary of the fatigue crack towards the bottom of the dimple along a line approximately coincident with the axis of the hole.

In the case of the Swiss sequence the fracture surface features used as a reference for crack growth measurements were those associated with the flights containing the maximum load of $+7{\cdot}5$ g (i.e. flights 48 and 150) and adjoining flights. These features had been used previously to determine the crack propagation characteristics of the first spar which failed during the F + W full-scale test (Reference 6). For all but one of the seven specimens tested under the Swiss sequence, measurements were made from crack depths of less than 1 mm, the smallest being $0{\cdot}47$ mm (BJ7IB). At smaller crack depths the features could not be identified. Figure 20 shows the basic crack depth/flights relationships for these specimens. The very good linear correlation between log. flights and log. crack depth which was reported in Reference 16 is also evident in Figure 20(*c*).

Unfortunately, no characteristic repeating pattern on the fracture surfaces could be identified for specimens tested under the Australian sequence, and this precluded crack growth measurements being made for this sequence using fractographic techniques.

No crack propagation studies were made on any of the front-flange specimens tested during this investigation, although such studies had been made previously (Reference 14) on this type of specimen tested under a simplified flight-by-flight loading sequence.

7. LIFE PREDICTIONS (Blind anchor-nut hole specimens)

The constant-amplitude fatigue tests on blind anchor-nut hole specimens (Figures 13 and 14) provided the basis for a set of S/N curves, the derivation of which is fully described in Appendix 2. These curves were used to predict the fatigue lives of such specimens under both the Australian and Swiss stress spectra at the various stress scaling factors. In every case a linear accumulation of fatigue damage was assumed.

Fatigue "cycles" within the Australian and Swiss sequences were derived from the occurrences of peaks and troughs using three different procedures.

(A) A one-pass range-mean-pair method (Reference 18) in which each range-mean-pair (as it was identified in the sequence) was used to directly calculate damage. In this case the load cycles were defined by the actual turning point values. An essential requirement for this procedure is the actual strain sequence.

(B) A range-mean-pair table (Table 7) generated simultaneously with the method used in (A) in which range-pairs, grouped into stress levels of equal intervals, formed an array of cells. Although many combinations of range-mean-pair stresses were counted within the boundaries of a particular cell, the individual stress values were not used for damage calculations; rather the stress values chosen were the average of the levels bounding the cell.

(C) A simulated Fatigue Meter count was produced from the range-mean-pair table, and fatigue damage calculated by successively combining the maximum peaks and minimum troughs in the stress sequence into groups of cycles with the same mean and alternating stresses. This method has been previously referred to as the "H_1 cumulative damage hypothesis" (References 19 and 20).

Table 8 indicates the fatigue lives calculated using the above procedures (A) to (C) for both the Australian and Swiss sequences and a range of stress scaling factors.

8. DISCUSSION

The long fatigue lives (and corresponding testing times) associated with specimens tested under the Australian sequence at low values of stress scaling factor, and the incidence of failures in the gripping areas of the specimens in such cases, precluded the direct comparison of experimental data under the Australian and Swiss sequences at stress scaling factors of less than 1·4 and less than 1·67 for the blind anchor-nut hole and front flange specimens respectively.

Tables 9 and 10 provide a comparison of the fatigue lives (at common stress scaling factors) for the dimpled bushed blind hole and front flange specimens under both the Australian and Swiss test sequences. For the blind hole specimens the ratio of Australian/Swiss experimentally determined lives is about two, while for the front flange specimens the ratio is greater, being in excess of 3·5 in the case of the interference-fit bolt specimens and almost five for the clearance-fit bolt specimens at a scaling factor of 1·67. It would thus appear that the relative effects of the two sequences on fatigue life are dependent on the "inherent" fatigue properties of the particular structural detail under consideration (in this case a "simple" geometric stress concentrator on the one hand, and a filled hole on the other where fretting could influence crack initiation) and the contributions of particular load levels in the two spectra to the total fatigue damage (i.e. the damage distribution) in each case.

On the assumption that the materials used for the two types of specimen have similar fatigue characteristics (although their values of fracture toughness – see Table 2(*c*) – are significantly different), the lives of these specimens under their respective spectra (i.e. Australian and Swiss) at a common scaling factor should provide an indication of the relative fatigue performance of each spectrum type/design detail combination. At a stress scaling factor of 1·67 the life of the dimpled blind hole specimen under the Australian spectrum is 20,000 flights (by interpolation from Figure 15)*, whereas for the front flange specimens under the Swiss spectrum the lives are 4,760 and 1,210 flights for the interference-fit and clearance-fit bolt types respectively. The numerical order of these lives is consistent with those from the full-scale wing tests at ARL and F + W (Reference 8) where the life at the blind hole under the Australian sequence was 33,667 flights; this being considerably greater than that at the no. 12 bolt hole under the Swiss sequence, i.e. 7,248 flights – a ratio (Australian/Swiss) of 4·6. For these tests on small specimens the ratios are 4·2 (for the interference-fit bolt case) and 16·5 (for the clearance-fit bolt case) respectively at a stress scaling factor of 1·67. At a scaling factor of 1·3 (which represents a limit for reasonable extrapolation of the curves in Figures 15 and 17) the ratio of Australian and Swiss (clearance-fit) lives is about three.

The relative severities of the two spectra can also be assessed by considering the fatigue life data in terms of the maximum stress in the sequences at various scaling factors. Figure 21 was derived from the data in Tables 3, 5 and 6. At high values of maximum stress similar specimens tested under the two spectra indicate only small differences in life, but at lower stresses there is a consistent trend for specimens tested under the Swiss spectrum to have longer lives than those tested under the Australian spectrum. This result is not surprising when the spectra are compared on the basis of common values of stress at 7·8 g and 7·5 g (Figure 22).

Table 8 indicates, for the particular type of specimen and stress spectra used in this investigation, that the lives predicted by each of the three procedures considered are not significantly different. Those predicted by Procedure (A) are plotted on Figure 15. The fatigue lives are underestimated at high stress scaling factors and overestimated at low stress scaling factors – by factors of up to about two in each case. Furthermore, as indicated in Table 9, the predictions suggest greater ratios (Australian/Swiss) in the lives to failure under the two spectra (i.e. from about 3 to 5) than those found experimentally (i.e. about 2). The lower ratios found experimentally may reflect a greater crack growth retardation effect under the maximum stress in the

* At this scaling factor the life of the spherical hole specimen is (by extrapolation) about 48,000 flights.

Australian sequence. Crack retardation effects were not incorporated in evaluating the predicted lives. These ratios of predicted lives are also greater than those presented in Reference 9 where, on a flights basis at the ARL-test spar failure location, they ranged between about 2 and 3 depending on the life prediction method adopted and the basic S/N data used. However, as indicated in Reference 8, the predicted lives are sensitive to the shapes of the S/N curves used for fatigue damage assessment. Whereas, in the present investigation these curves were derived from constant-amplitude tests on the actual detail under consideration, those used for the damage calculations in Reference 9 were based firstly on a functional representation of data from fatigue tests on full-scale aluminium alloy structures and, secondly, from fatigue tests on small circumferentially notched specimens of $K_t = 2{\cdot}8$.

It is of interest to note that the current fatigue tests under the flight-by-flight sequences support the findings of previous investigations regarding:

(i) the detrimental effects on fatigue life of a dimple in an otherwise spherical-base blind hole (Reference 5) and,

(ii) the advantages of using interference-fit compared with clearance-fit fasteners (Ref. 14). At a stress scaling factor of 1·67 the life ratios (interference/clearance fit bolt) under the Australian and Swiss spectra are about 3·0 and 3·9 respectively.

9. CONCLUSIONS

1. At stress levels equivalent to those in the Australian and Swiss full-scale fatigue tests the fatigue lives of specimens representing the types of structural details at which the failures occurred (blind anchor nut hole – Australian, and front flange bolt hole – Swiss) are greater under the Australian stress spectrum than under the Swiss stress spectrum.

2. Under both the Australian and Swiss stress spectra, the lives of front-flange bolt hole specimens incorporating interference-fit bolts were between 3 and 4 times greater than those with clearance-fit bolts.

3. At a common stress scaling factor the grouping together of the two different stress spectra and the two different types of specimens indicates a life ratio (Australian/Swiss flights) of between 4·2 and 16·5, depending on whether the front flange specimens were fitted with interference-fit or clearance-fit bolts.

4. The life ratios of 4·2 and 16·5 compare with a ratio of 4·6 which resulted from a comparison of the Mirage full-scale wing fatigue tests at ARL and F + W.

5. For the blind anchor-nut hole specimens the predicted fatigue lives were less than those obtained experimentally at high stress scaling factors, but at low stress scaling factors the converse was the case.

6. Again for the blind anchor-nut hole specimens, the ratios of the predicted lives to failure (Australian/Swiss) were greater than those found experimentally

ACKNOWLEDGEMENTS

The authors wish to acknowledge the assistance which they received from Mr D. Maclean during the preparation of the computer control tapes, and that provided by Mr W. F. Lupson, Mr F. G. Harris and Mr A. S. Machin in the conduct of the fatigue tests and in carrying out the statistical analysis of the data. Crack growth measurements were made by Mr R. A. Pell and his help in this aspect of the investigation is also gratefully acknowledged

REFERENCES

1. Howard, P. J., Patching, C. A. and Payne, A. O. Life estimation by parametric analysis. *Problems with fatigue in aircraft.* Proceedings of the Eighth ICAF Symposium. [Edited by J. Branger and F. Berger]. Emmen, 1975, pp. 4.3/1–4.3/28.

2. Howard, P. J. Development of a load sequence for a structural fatigue test. *Aircraft structural fatigue. Dept. Defence Aero. Res. Labs.* Structures Report 363/Materials Report 104, April 1977, pp. 137–148.

3. Bruton, R. A. Failures resulting from a fatigue test on a Mirage IIIO wing. *Dept. Defence Aero. Res. Labs.* Structures Tech. Memo. 319, July 1980.

4. Anderson, B. E., and Goldsmith, N. T. Prediction of crack propagation in Mirage wing fatigue test spar. *Dept. Defence Aero. Res. Labs.* Structures Note 448/Materials Note 124, April 1978.

5. Mann, J. Y., Harris, F. G., and Machin, A. S. Notched specimen fatigue tests relating to the ARL Mirage fatigue test spar boom fracture. *Dept. Defence Aero. Res. Labs.* Structures Tech. Memo. 279, September 1978.

6. Goldsmith, N. T. Fractographic examinations relevant to the F+W Mirage fatigue test. *Dept. Defence Aero. Res. Labs.* Materials Tech. Memo. 371, August 1978.

7. Howard, P. J., Sparrow, J. G., and Thomson, M. R. Strain distributions in the Mirage main spar. *Dept. Defence Aero. Res. Labs.* Structures Note 464, October 1980.

8. Grandage, J. M. A reassessment of the ARL and Swiss Mirage fatigue test lives. *Dept. Defence Aero. Res. Labs.* Structures Note 468, December 1980.

9. Graham, A. D., Grandage, J. M., Rider, C. K., and Thomson, M. R. Comparison of the ARL and Swiss Mirage fatigue test lives using ARL strain survey data. *Dept. Defence Aero. Res. Labs.* Structures Note 478, July 1981.

10. Grandage, J. M., and Howard, P. J. Mirage IIIO wing fatigue test — development of the load sequence. *Dept. Defence Aero. Res. Labs.* Structures Note 460, June 1980. (CONFIDENTIAL).

11. Rhomberg, H. Review of Swiss investigations on aeronautical fatigue — period June 1975 to May 1977. *F+W Emmen* Rep. No. TA-346, 1977.

12. Anderson, B. E. Preliminary assessment to September 1977 of the panel failure in the F+W Mirage fatigue test. *Dept. Defence Aero. Res. Labs.* Structures Tech. Memo. 288, January 1979.

13. Mann, J. Y., and Harris, F. G. An investigation of the fatigue performance of three types of aircraft skin/spar boom fastening system. Part 1: Constant-amplitude fatigue tests. *Dept. Defence Aero. Res. Labs.* Structures Report 350, September 1974.

14. Mann, J. Y., Machin, A. S., Lupson, W. F., and Pell, R. A. The use of interference-fit bolts or bushes and hole cold expansion for increasing the fatigue life of thick-section aluminium alloy bolted joints. *Dept. Defence Aero. Res. Labs.* Structures Note 490, August 1983.

15. Sparrow, J. G. Tripartite Mirage programme report — December 1980. *Dept. Defence Aero. Res. Labs.* Structures Tech. Memo. 326, February 1981.

16. Mann, J. Y., Pell, R. A., and Machin, A. S. Fatigue crack propagation in Mirage IIIO wing main spar specimens and the effects of spectrum truncation on life. *Dept. Defence Aero. Res. Labs.* Structures Report 405, July 1984.

17. Pell, R. A. Unpublished work.

18. Fraser, R. C. A one-pass method for counting range mean pair cycles for fatigue analysis. *Dept. Defence Aero. Res. Labs.* Structures Note 454, June 1979.

19. Payne, A. O. Determination of the fatigue resistance of aircraft wings by full-scale testing. *Full-scale fatigue testing of aircraft structures.* [Editors: F. J. Plantema and J. Schijve]. Oxford: Pergamon Press, 1961, pp. 76–132.

20. Finney, J. M., and Mann, J. Y. Fatigue behaviour of notched aluminium alloy specimens under simulated random gust loading with and without ground-to-air cycles of loading. *Fatigue of aircraft structures.* [Editors: W. Barrois and E. L. Ripley]. Oxford: Pergamon Press, 1963, pp. 151–177.

21. Mann, J. Y. The influence of mean stress and stress concentrators on the fatigue properties of 7178-T6 aluminium alloy. *Dept. Supply Aero. Res. Labs.* Report ARL/SM.327, Nov. 1970.

22. Howard, P. J. Fatigue damage due to gust loading of Mirage IIIO aircraft. *Dept. Defence Aero. Res. Labs.* Structures Note 428, June 1976.

APPENDIX 1

Derivation of test stresses for front flange specimens

The stress at 7·5 g was derived from strains measured at gauge 1·4T during the 1979 strain survey of the left-hand Swiss Mirage test wing. This gauge was located at the inner surface of the lower front flange of the main spar between bolt hole no. 14 and the spar web, and a multiplying factor of 1·2 was used to estimate the strain at the Swiss failure location (hole no. 12). Two different methods were used to estimate the strain at 7·5 g, and the value of 235 MPa adopted for this investigation was an average of the two. The first was determined directly from the actual numerical value of strain at 5 g using the ratio 7·5 (g)/5 (g) and resulted in a strain of 3240 microstrain (stress 237 MPa). The second method was based on the average microstrain per g from the 1 g to 5 g increment (Ref. 15) and resulted in a strain of 3201 microstrain (stress 234 MPa).

APPENDIX 2

Development of a family of S/N curves for fatigue life estimates

A basic requirement for estimating fatigue lives under the different loading conditions used in this investigation was S/N data under various combinations of alternating stress (S_a) and mean stress (S_m). However, as no comprehensive fatigue data for a detail representing the blind anchor nut were available, the following procedure was used to generate a data bank for life estimation purposes.

The constant-amplitude data for bushed dimpled hole (BDH) specimens at $S_m = 48$ MPa (6·95 ksi[◊]) listed in Table 4 and shown on Figure 14 was adopted as the primary base for the development of a family of S/N curves. These data were supplemented by similar data from tests on blind hole Chobert Rivet (CR) joint specimens at mean stresses of 35 MPa (5·1 ksi) and 87 MPa (12·6 ksi) taken from Reference 13. Both the BDH and the CR specimens were from the same batch of 2L.65 test material. These three sets of data are shown plotted (using log–log scales) on Figure 23, together with the best fit S/N straight lines in each case – lines X, Y and Z. For simplicity in subsequent analysis, a very minor correction was made to these lines to ensure that all three intersected at the point $S_a = 228$ MPa (33·1 ksi), $N = 3892$ cycles.

On the assumption that, at constant lives between mean stresses of 5·1 and 12·6 ksi, the alternating and mean stresses were linearly related, a simple process of interpolation provided a line representing the CR S/N curve at a mean stress of 6·95 ksi. Having the S/N lines of both the BDH and CR specimens at $S_m = 6·95$ ksi, the S/N lines for the BDH specimens at mean stresses of 5·1 and 12·6 ksi were determined (at constant S_a) by multiplying the log lives of the CR specimens at 5·1 and 12·6 ksi by the ratio:

$$\frac{\text{log life (BDH) at 6·95 ksi}}{\text{log life (CR) at 6·95 ksi}}$$

The six S/N lines, three experimental and three derived, are shown on Figure 23, and the appropriate equations for the BDH specimens are as follows:*

For

$$S_m = 5·1 \text{ ksi},$$

$$\text{log life} = 28·4675 - 5·5040 (\log S_a) \quad (1)$$

For

$$S_m = 6·95 \text{ ksi},$$

$$\text{log life} = 26·7715 - 5·1288 (\log S_a) \quad (2)$$

For

$$S_m = 12·6 \text{ ksi},$$

$$\text{log life} = 21·7615 - 4·0203 (\log S_a) \quad (3)$$

[◊] For this analysis all stress values were in ksi units. 1 ksi = 6·8948 MPa.

* The numbers of decimal places in the equations which follow are not indicative of the precision of the fitted lines.

A partial S_a/S_m diagram was then constructed for mean stresses of between 5·1 and 12·6 ksi and lives of from 10^4 to 10^7 cycles. The slopes of the various life lines in this interval of mean stress were matched against those for notched specimens of $K_t = 1·6$ in Reference 21, and the lines of constant life on this diagram extrapolated to mean stresses of −14 MPa (−2·0 ksi) in one direction and about +172 MPa (+25 ksi) in the other direction. From this S_a/S_m diagram further S/N curves were derived for the corresponding range of mean stresses.

As stated in Appendix 1 to Reference 22 the relationship between S_a, S_m and N for a series of straight lines radiating from a point can be expressed in the form:

$$\log N = \log N_o + (\log N_1 - \log N_o)\frac{\log S_{ao} - \log S_a}{\log S_{ao} - \log (f(S_m))} \quad (4)$$

Where:

S_{ao}, N_o correspond to the intersection point of the various lines (in this case 228 MPa (33·1 ksi) and 3892 cycles respectively), and N_1 = a reference life used for the derivation of $f(S_m)$ (in this case taken as 10^5 cycles).

$f(S_m)$ was obtained by cross plotting values of S_a at 10^5 cycles against $\log (S_m + C)$ and adjusting the constant 'C' until the best fit straight line relationship between these two parameters was obtained. The resulting equation ($C = 22$) was:

$$f(S_m) = 66·2674 - 33·4236 \log (S_m + 22) \quad (5)$$

Substitution of (5) into (4) and providing numerical values for S_{ao} and N_o resulted in the required formulation:

$$\log N = 3·5902 + 1·4098\left[\frac{1·5198 - \log S_a}{1·5198 - \log (66·2674 - 33·4236 \log (S_m + 22))}\right] \quad (6)$$

A test for the validity of this equation is its ability to reproduce the S–N line for the BDH specimens at a mean stress of 6·95 ksi. The values of life at alternating stresses of 33·1 and 6·0 ksi from equations (2) and (6) are as follows:

	Cycles (N)		
S_a (ksi)	Equation (2)	Equation (6)	Equation (7)
33·1	3892	3892	3892
6·0	24,779,926	21,820,638	24,744,605

Although the difference in calculated lives is relatively small at the alternating stress of 6·0 ksi, it can be made negligible by a minor correction to the numerical value of the constant 'C' in equation (6), i.e. by substituting 21·68 instead of 22. Equation (6) then becomes:

$$\log N = 3·5902 + 1·4098\left[\frac{1·5198 - \log S_a}{1·5198 - \log (66·2674 - 33·4236 \log (S_m + 21·68))}\right] \quad (7)$$

The lives for alternating stresses of 33·1 and 6·0 ksi and mean stress of 6·9 ksi calculated using equation (7) are also given above.

Equation (7) was then used to generate a complete set of S/N curves covering the mean stresses of interest for lives exceeding 3892 cycles, and representative lines are shown on Figure 24. For lives of less than 3892 cycles the assumption was made that the effects of mean stress were negligible and, thus, a common relationship existed between life and alternating stress having

as its upper limit the co-ordinates UTS = 510 MPa (74·0 ksi), N = 0·5 cycles. The equation for this part of the diagram is:

$$\log \text{life} = 53{\cdot}9261 - 11{\cdot}1367 \, (\log S_a) \tag{8}$$

Finally, equation (7) was used to generate an S_a/S_m diagram for bushed dimpled-hole specimens at various lives, part of which is reproduced in Figure 25.

TABLE 1

Sequence of the 24 "typical" flights (TF) in F + W 200-flight test loading sequence (Reference 6)

Flights				
1 to 40	41 to 80	81 to 120	121 to 160	161 to 200
1 TF14	41 TF14	81 TF14	121 TF9	161 TF22
2 TF10	42 TF12	82 TF10	122 TF5	162 TF4
3 TF6	43 TF21	83 TF15	123 TF5	163 TF12
4 TF11	44 TF6	84 TF23	124 TF16	164 TF11
5 TF15	45 TF17	85 TF24	125 TF13	165 TF3
6 TF16	46 TF13	86 TF21	126 TF17	166 TF14
7 TF17	47 TF10	87 TF12	127 TF21	167 TF11
8 TF21	[48 TF2]	88 TF17	128 TF22	168 TF9
9 TF23	49 TF11	89 TF19	129 TF15	169 TF11
10 TF13	50 TF21	90 TF16	130 TF17	170 TF1
11 TF11	51 TF23	91 TF6	131 TF21	171 TF14
12 TF22	52 TF13	92 TF11	132 TF12	172 TF4
13 TF24	53 TF23	93 TF13	133 TF24	173 TF21
14 TF5	54 TF15	94 TF11	134 TF14	174 TF10
15 TF12	55 TF3	95 TF20	135 TF13	175 TF13
16 TF18	56 TF19	96 TF14	136 TF24	176 TF15
17 TF14	57 TF14	97 TF7	137 TF7	177 TF21
18 TF5	58 TF7	98 TF23	138 TF23	178 TF17
19 TF23	59 TF15	99 TF4	139 TF16	179 TF23
20 TF13	60 TF12	100 TF7	140 TF22	180 TF15
21 TF3	61 TF24	101 TF5	141 TF14	181 TF6
22 TF8	62 TF23	102 TF20	142 TF10	182 TF24
23 TF21	63 TF16	103 TF11	143 TF21	183 TF11
24 TF17	64 TF21	104 TF17	144 TF4	184 TF17
25 TF11	65 TF22	105 TF18	145 TF15	185 TF24
26 TF13	66 TF19	106 TF5	146 TF5	186 TF4
27 TF15	67 TF13	107 TF10	147 TF15	187 TF21
28 TF24	68 TF22	108 TF13	148 TF24	188 TF12
29 TF21	69 TF21	109 TF4	149 TF12	189 TF20
30 TF11	70 TF8	110 TF12	[150 TF2]	190 TF10
31 TF23	71 TF24	111 TF22	151 TF11	191 TF16
32 TF22	72 TF17	112 TF13	152 TF23	192 TF5
33 TF7	73 TF10	113 TF23	153 TF8	193 TF14
34 TF11	74 TF9	114 TF11	154 TF11	194 TF23
35 TF22	75 TF15	115 TF19	115 TF23	195 TF13
36 TF6	76 TF13	116 TF10	156 TF13	196 TF23
37 TF10	77 TF16	117 TF15	157 TF9	197 TF17
38 TF14	78 TF12	118 TF18	158 TF22	198 TF15
39 TF16	79 TF14	119 TF9	159 TF17	199 TF14
40 TF8	80 TF21	120 TF11	160 TF8	200 TF16

The flights containing normal accelerations of 6·5 g and greater are underlined and the maximum values applied in such flights are listed below.

TF1	TF2	TF3	TF4	TF5
6·5 g	7·5 g	6·5 g	7·0 g	6·5 g

TABLE 2

Properties of test materials

(a) Chemical composition (%)

Element	‡Specification A7-U4SG (2214)	British Standard 2L.65: 1959	British Standard L168: 1978	Test material GR
Cu	3·9–5·0	3·8–4·8	3·9–5·0	4·29
Mg	0·2–0·8	0·55–0·85	0·2–0·8	0·43
Mn	0·4–1·2	0·4–1·2	0·4–1·2	0·76
Fe	0·30 max.	1·0 max.	0·50 max.	0·23
Si	0·5–1·2	0·6–0·9	0·5–0·9	0·74
Ti	0·15 max.	0·3 max.	0·15 max.	*not analyzed*
Cr	0·10 max.		0·10 max.	0·01
Zn	0·25 max.	0·2 max.	0·25 max.	<0·20

(b) Static tensile

Property	‡Specification A7-U4SG (2214)	British Standard 2L.65: 1959	Test material BJ	British Standard L168: 1978	Test material GR
0·1% proof stress (MPa)	—	432	457 (sd 12)	—	466 (sd 10)
0·2% proof stress (MPa)	390	—	463 (sd 13)	440	474 (sd 12)
Ultimate tensile stress (MPa)	450	494	510 (sd 10)	490	524 (sd 12)
Elongation (%)	5	8	11·5 (sd 1)	7	11 (sd 2)
0·1% PS/Ult	—	—	0·90	—	0·89

sd = standard deviation.

(c) Fracture toughness

Fracture toughness, K_{1C} (MPa.m$^{\frac{1}{2}}$)		
Test material BJ (specimen thickness 25 mm)	Test material GR	
	Specimen thickness 25 mm	Specimen thickness 19 mm
25·9◊	34·5*	32·0†

◊ Average of seven specimens from four bars.
* Average of two specimens from one bar.
† Average of five specimens from five bars.
‡ *Conditions de controle des produits lamines en alliages d'aluminium utilises dans les constructions aerospatiales.* Ministere de la Defense, Direction Technique des Construction Aeronautiques AIR 9048, Edition No. 1, 26 December, 1978, p. 91. [Specification A7-U4SG superseded A-U4SG, the material from which the spars were manufactured].

TABLE 3

Stresses at maximum 'g' loads of sequences for various stress scaling factors

Stress scaling factor	Australian (+7·8 g)		Swiss (+7·5 g)	
	Gross area (MPa)	Nett area (MPa)	Gross area (MPa)	Nett area (MPa)
Blind anchor-nut hole specimens				
2·6	346	403	—	—
2·4	319	372	—	—
2·2	293	341	420	490
2·0	266	310	382	445
1·8	239	279	344	401
1·5	200	233	287	334
1·4	186	217	267	311
1·0	133	155	191	223
Front flange bolt hole specimens				
2·23	326	364	—	—
1·67	245	273	352	393
1·34	195	218	282	315
1·23	179	200	258	288
1·12	163	182	235	262
1·0	146	163	211	235

TABLE 4

Blind anchor-nut hole specimens — Constant-amplitude fatigue lives (S_m = 48 MPa; 6·95 ksi)

Specimen number (BJ)	Alternating stress range (MPa; ksi)	Cycles
Unbushed spherical hole (10)		
20D	259; 37·5	36,400
6F	259; 37·5	35,700
5C	259; 37·5	46,200
4H	222; 32·23	112,200
20I	222; 32·23	146,600
12G	222; 32·23	196,200
13D	207; 30·0	110,800
15H	207; 30·0	863,100
8I	203; 29·39	1,918,300
14F	203; 29·39	2,199,100
Unbushed dimpled hole (6)		
9H	259; 37·5	82,300
17I	222; 32·23	259,000
15H	207; 30·0	68,000
14G2	190; 27·5	428,100
18E2	190; 27·5	7,644,000
10F	190; 27·5	9,425,000
Bushed dimpled hole (11)		
7B	259; 37·5	88,700
1D	222; 32·23	256,000
11I	207; 30·0	140,700
13C	190; 27·5	247,800
14B	172; 25·0	922,800
15I	155; 22·5	683,600
17J	155; 22·5	2,929,900
19C	121; 17·5	7,962,200
20F	121; 17·5	1,603,600
18H	121; 17·5	4,599,000
2I	97; 14·0	19,767,000 UB

TABLE 5

Blind anchor-nut bushed hole specimens — fatigue lives under Australian and Swiss sequences

Specimen		Stress scaling factor	Average cyclic frequency (Hz)	Life to failure (flights)	Log average life (flights)	s.d. of log life
Number BJ	Type					
Australian sequence						
16D	SH	2·6	4·6	2,747	3,130	0·080
9I	SH	2·6	1·3	3,564		
10G	SH	2·4	1·3	6,564		
20I	SH	2·2	4·6	9,546	10,730	0·072
18E1	SH	2·2	1·3	12,065		
18F	SH	2·0	4·6	13,701	13,440	0·013
14G1	SH	1·96	1·1	13,132		
13I	SH	1·8	4·6	22,993		
8H	SH	1·8	4·6	34,932	31,620	0·123
16E1	SH	1·8	4·6	39,363		
8DB	DH	2·6	4·6	4,990		
9GB	DH	2·2	4·6	7,990		
16E2	DH	2·2	1·1	8,046	8,910	0·079
13D	DH	2·2	4·6	10,990		
12G	DH	2·0	1·1	12,564		
7EB	DH	1·8	4·6	12,643		
9BB	DH	1·8	4·6	12,703	13,990	0·075
10JA	DH	1·8	4·6	17,064		
7F	DH	1·4	4·6	29,185		
12D	DH	1·4	4·6	52,292	43,230	0·148
11JB	DH	1·4	4·6	52,953		
Swiss sequence						
19E	SH	2·2	9·3	847		
1F	SH	1·8	9·3	8,949	9,810	0·057
12F	SH	1·8	9·3	10,752		
10IB	DH	2·2	9·3	647	700	0·044
15JB	DH	2·2	9·3	749		
10EB*	DH	1·8	9·3	5,847		
7IB	DH	1·8	9·3	6,749	7,160	0·087
6HB	DH	1·8	9·3	7,047		
7C	DH	1·8	9·3	9,447		
7HB	DH	1·4	9·3	19,749		
9DB	DH	1·4	9·3	21,749	21,220	0·027
4GB	DH	1·4	9·3	22,247		
6JB	DH	1·0	9·3	55,247		
4JB	DH	1·0	9·3	65,785	63,860	0·058
6C	DH	1·0	9·3	71,647		

SH — spherical hole; DH — dimpled hole.

* High compressive load applied at 5,370 flights; not included in analysis.

TABLE 6

Front flange bolt hole specimens — fatigue lives under Australian and Swiss sequences

Specimen		Stress scaling factor	Average cyclic frequency (Hz)	Life to failure (flights)	Failure hole no.	Log. average life (flights)	s.d. of log. life
Number GR	Type						
Australian sequence							
15A	I	2·23	4·6	4,631	4	6,000	0·159
21A	I	2·23	4·6	7,765	4		
26A	I	2·23	4·6	8,800	Grip*		
18A	I	1·67	4·6	14,438	5	17,560	0·120
25A	I	1·67	4·6	21,202	Grip*		
11A	I	1·67	4·6	21,368	2		
15E	C	2·23	4·6	1,378	2	1,500	0·052
18C	C	2·23	4·6	1,631	2		
12C	C	1·67	4·6	5,373	4	5,810	0·035
26C	C	1·67	4·6	5,773	2		
14C	C	1·67	4·6	6,307	2		
24C	C	1·34	4·6	12,300	4	13,670	0·042
16C	C	1·34	4·6	13,932	2		
20C	C	1·34	4·6	14,894	2		
Swiss sequence							
12A	I	1·67	9·3	3,149	2	4,760	0·206
19A	I	1·67	9·3	3,821	2		
23A	I	1·67	9·3	4,549	4		
14A	I	1·67	9·3	9,351	1		
20A	I	1·34	9·3	67,549	Grip*		
24A	I	1·23	9·3	102,656	unbroken		
21C	C	1·67	9·3	851	4	1,210	0·133
23C	C	1·67	9·3	1,447	2		
22C	C	1·67	9·3	1,448	4		
25C	C	1·23	9·3	5,750	4	6,040	0·030
13E	C	1·23	9·3	6,350	4		
3A	C	1·12	9·3	13,349	2	14,530	0·052
4B	C	1·12	9·3	15,817	4		

C — Clearance-fit bolt; I — Interference-fit bolt.

* Not included in analysis.

TABLE 7(a)

Range-mean-pair table for Australian Mirage spectrum. Stresses at front flange bolt hole number 12

Stress (MPa)	Level	1	2	3	4	5	6	7	8	9	10	11	12	13	14	15	16	17	18	19	20	21	22	23	24	25
51·8	1	0																								
43·2	2	0	0																							
34·5	3	0	0	0																						
25·9	4	0	0	0	0																					
17·3	5	0	0	0	0	0																				
8·6	6	0	0	0	0	0	0																			
0	7	0	0	0	0	0	0	0																		
8·6	8	0	0	0	0	0	0	0	0																	
17·3	9	0	0	0	0	0	0	0	0	0																
25·9	10	0	0	0	0	0	0	43	431	12	0															
34·5	11	0	0	0	0	0	0	60	2256	1253	1	0														
43·2	12	0	0	1	0	11	374	4396	17607	909	1237	540	0													
51·8	13	0	0	0	11	48	1019	3188	3632	717	983	341	2	0												
60·5	14	0	0	1	7	86	588	513	482	764	537	742	338	23	0											
69·0	15	0	0	0	6	55	160	72	322	687	315	326	780	120	6	0										
77·9	16	0	0	1	7	30	80	59	355	589	253	271	244	382	171	0	0									
86·2	17	0	0	0	2	6	23	64	228	368	148	141	132	253	117	29	0	0								
95·2	18	0	0	2	7	7	38	24	250	306	70	80	152	126	118	143	31	2	0							
103·4	19	0	0	2	1	11	25	16	253	184	30	11	69	127	79	118	132	23	19	0						
112·4	20	0	2	2	13	15	14	32	209	226	12	2	62	3	22	9	34	68	53	0	0					
120·7	21	0	0	0	0	0	10	71	183	123	10	1	24	64	77	62	11	76	122	12	16	0				
129·6	22	0	0	7	9	14	25	141	212	51	2	0	10	1	12	0	10	1	5	21	44	16	0			
137·9	23	0	3	4	7	2	12	30	19	67	0	0	10	1	1	0	0	1	5	5	4	3	29	0		
146·9	24	0	5	6	1	0	8	6	0	6	0	0	0	0	0	0	0	0	0	1	0	0	5	1	0	
155·8	25	0	1	0	0	0	0	0	0	0	0	0	0	0	0	0	0	0	0	0	0	0	0	0	0	0

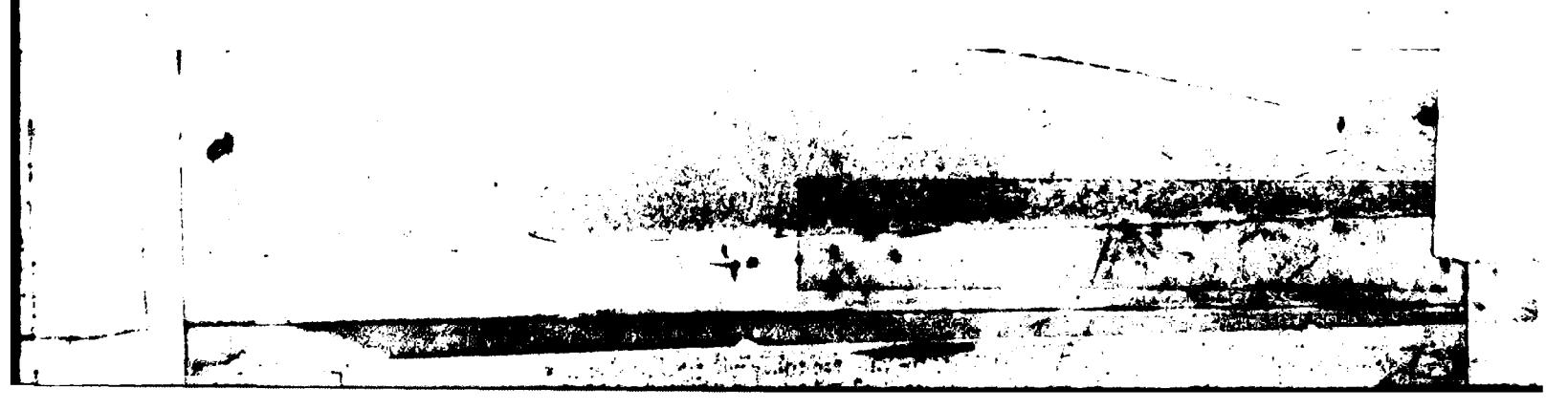

TABLE 7(b)

Range-mean-pair table for F + W spectrum. Stresses at front flange bolt hole number 12

Stress (MPa)	Level	1	2	3	4	5	6	7	8	9	10	11	12	13	14	15	16	17	18	19	20	21
96·5	1	0																				
80·7	2	0	0																			
64·3	3	0	0	0																		
48·3	4	0	0	0	0																	
32·1	5	0	0	0	0	0																
16·1	6	0	0	0	0	0	0															
0	7	0	0	0	0	0	0	446														
16·1	8	0	0	0	0	0	0	4177	4458													
32·1	9	0	0	0	0	0	0	430	1573	356												
48·3	10	0	0	0	0	0	0	298	765	349	0											
64·3	11	0	0	0	0	4	0	126	822	393	0	0										
80·7	12	0	0	0	0	2	0	230	358	236	146	5	0									
96·5	13	0	0	0	0	5	0	147	275	124	230	10	20	0								
112·4	14	0	0	0	0	0	0	158	330	29	50	30	0	19	0							
128·9	15	0	0	0	0	2	0	177	116	38	57	52	20	21	0	20						
144·8	16	0	0	0	0	52	0	72	57	0	1	0	0	0	0	0	0					
160·7	17	0	0	1	14	38	0	28	6	18	6	0	0	0	0	0	0	0				
177·2	18	0	0	0	0	14	0	0	0	0	0	0	0	0	0	0	0	0	0			
193·1	19	0	3	10	0	1	0	1	3	0	0	0	0	0	0	0	0	0	0	0		
208·9	20	1	2	3	0	0	0	0	0	0	0	0	0	0	0	0	0	0	0	0	0	
224·8	21	1	1	0	0	0	0	0	0	0	0	0	0	0	0	0	0	0	0	0	0	0

TABLE 8

Blind anchor-nut, dimpled bushed hole specimens — comparison of experimental and predicted lives

Stress scaling factor	Experimental life (flights)	Predicted life by procedures:					
		(A)		(B)		(C)	
		Flights	Life ratio	Flights	Life ratio	Flights	Life ratio
Australian sequence							
2·6	4,990*	2,390	2·09	2,380	2·10	2,940	1·70
2·2	8,907◊	5,190	1·72	5,160	1·73	6,170	1·44
2·0	12,564*	8,330	1·51	8,290	1·52	9,730	1·29
1·8	13,994◊	14,500	0·97	14,500	0·97	16,600	0·84
1·4	43,234◊	62,700	0·70	62,300	0·69	68,600	0·63
1·0	No tests	595,000	—	588,000	-	617,000	-
Swiss sequence							
2·2‡	698†	1,240	0·56	1,230	0·57	1,160	0·60
2·0	No tests	2,520	-	2,480	-	2,390	-
1·8	7,159#	4,980	1·44	4,840	1·48	4,690	1·53
1·4	21,220◊	18,700	1·13	18,200	1·17	17,700	1·20
1·0	63,857◊	128,000	0·50	126,000	0·51	121,000	0·53

* One result.

† Average of 2 tests.

◊ Average of 3 tests.

\# Average of 4 tests.

‡ Not considered in analysis because of unrealistically high +7·5 g stress.

$$\text{Life ratio} = \frac{\text{Experimental life}}{\text{Predicted life}}$$

TABLE 9

Blind anchor-nut, dimpled bushed hole specimens — ratios of lives under Australian (Au) and Swiss (Sw) sequences

Stress scaling factor	Au/Sw (experimental)	Au/Sw (predicted from Table 8)		
		Procedure (A)	Procedure (B)	Procedure (C)
2·2◊	12·76	4·19	4·20	5·32
1·8	1·96	2·91	3·00	3·54
1·67	2·0*	...	—	—
1·4	2·04	3·35	3·42	3·88
1·0	—	4·65	4·67	5·10

* Lives interpolated from Figure 15.
◊ Not considered in analysis because of unrealistically high +7·5 g stress in Swiss sequence.

TABLE 10

Front flange bolt hole specimens — ratios of lives under Australian (Au) and Swiss (Sw) sequences

Stress scaling factor	Au/Sw (experimental)
Interference-fit bolts	
1·67	3·69
Clearance-fit bolts	
1·67	4·79
1·4◊	3·4

◊ Lives interpolated from Figure 17.

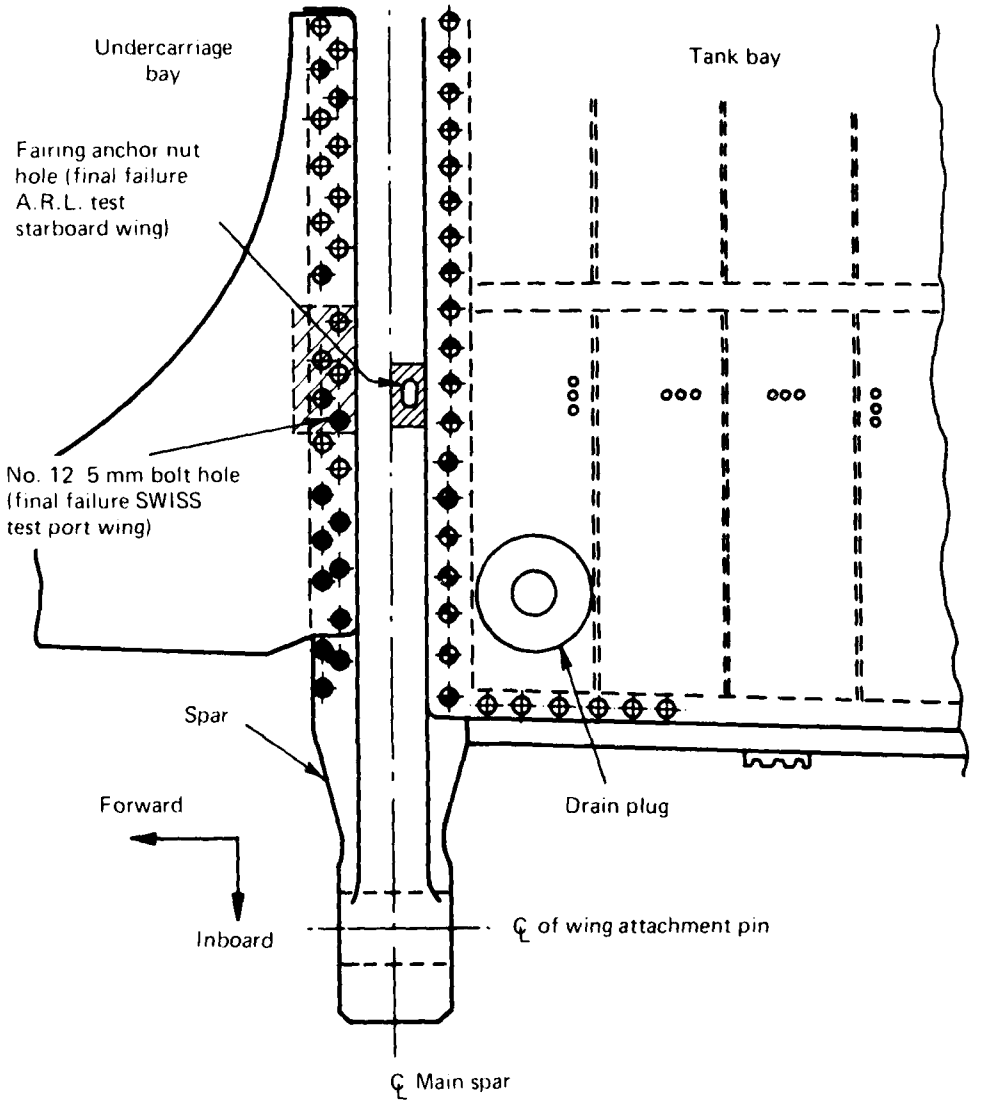

FIG. 1 MIRAGE PORT WING VIEWED FROM LOWER SURFACE

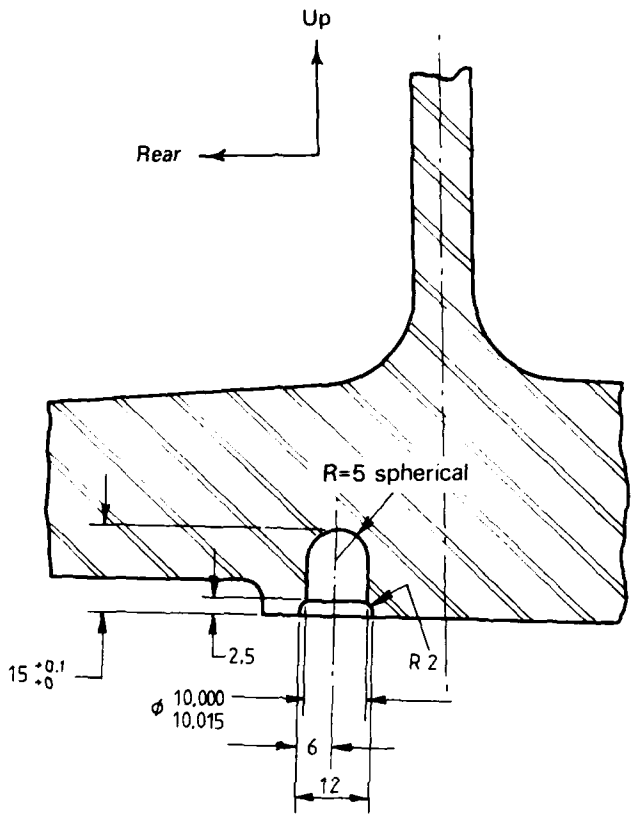

(a) Detail from Avions Marcel Dassault Drawing No. MIR. IIIE-113/3F.1

(b) Fatigue fracture (Ref. 3)

FIG. 2 FATIGUE FAILURE IN SPAR OF ARL TEST WING

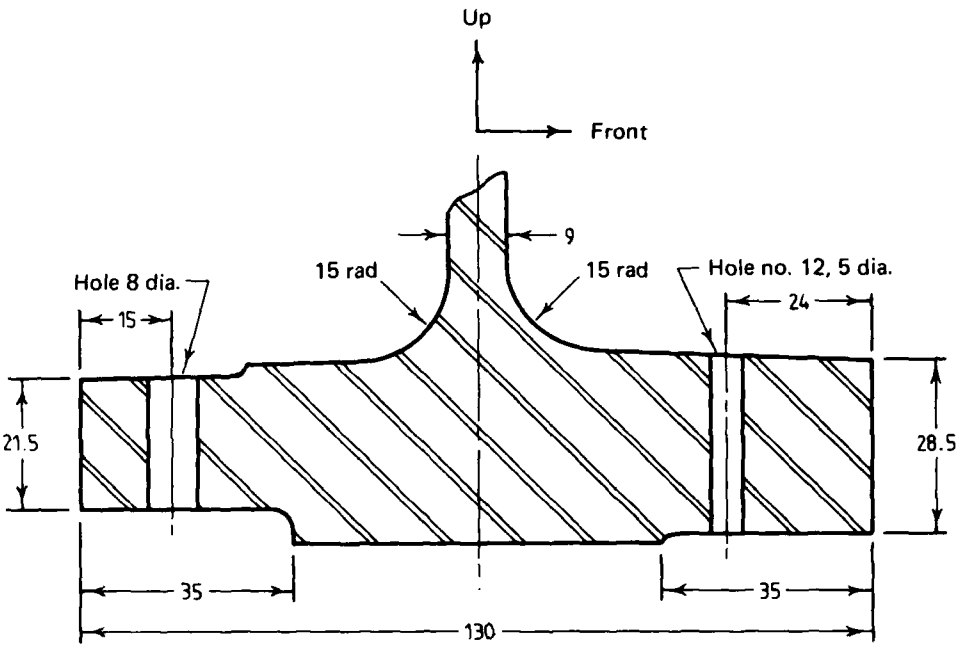

(a) Section through no. 12 bolt hole in front flange

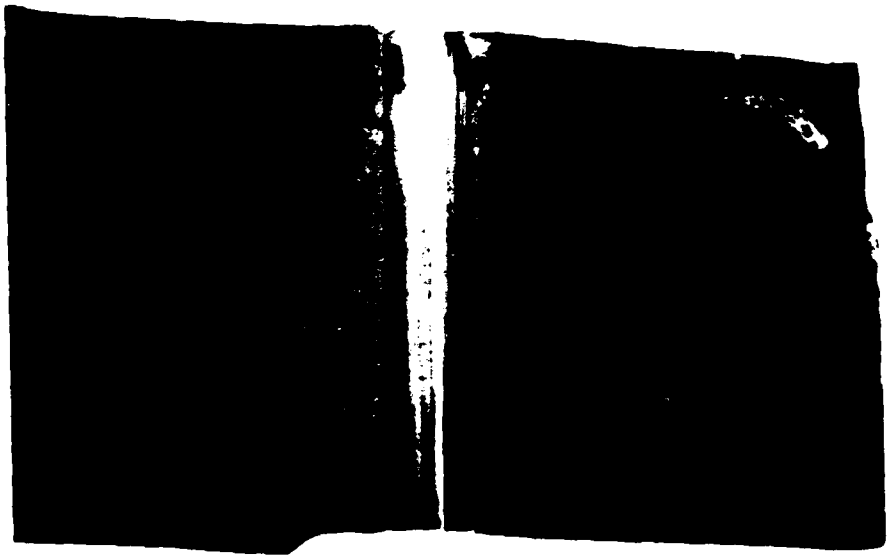

(b) Fatigue fracture at bolt hole no. 12 (Ref. 6)

FIG. 3 FATIGUE FAILURE IN SPAR OF F+W TEST WING

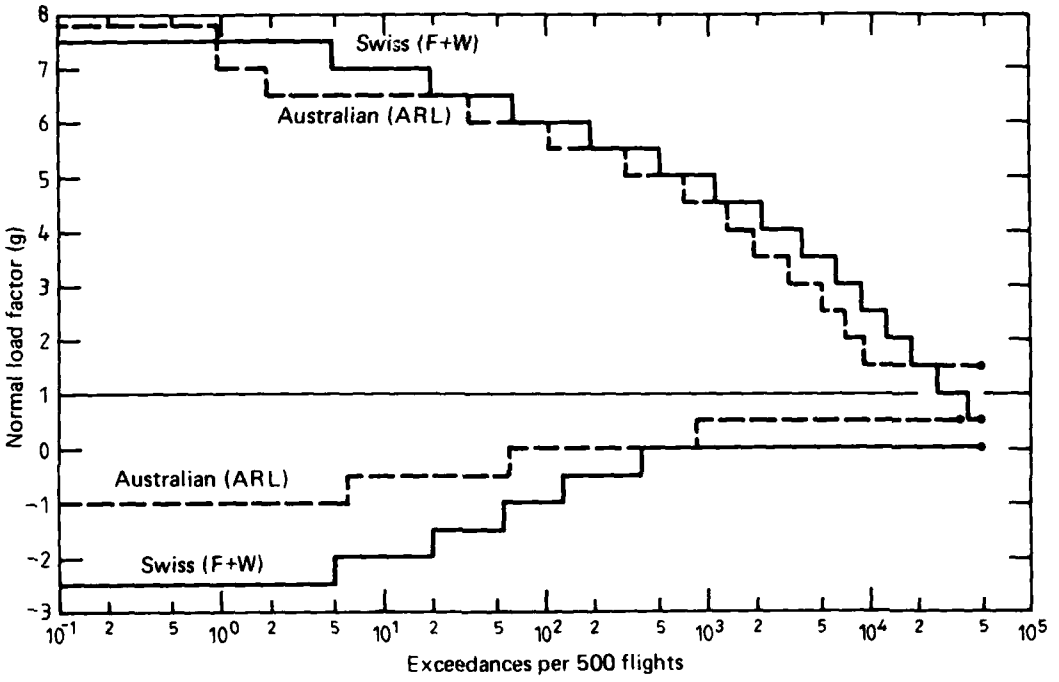

FIG. 4 ARL AND F+W FATIGUE TEST LOAD SPECTRA

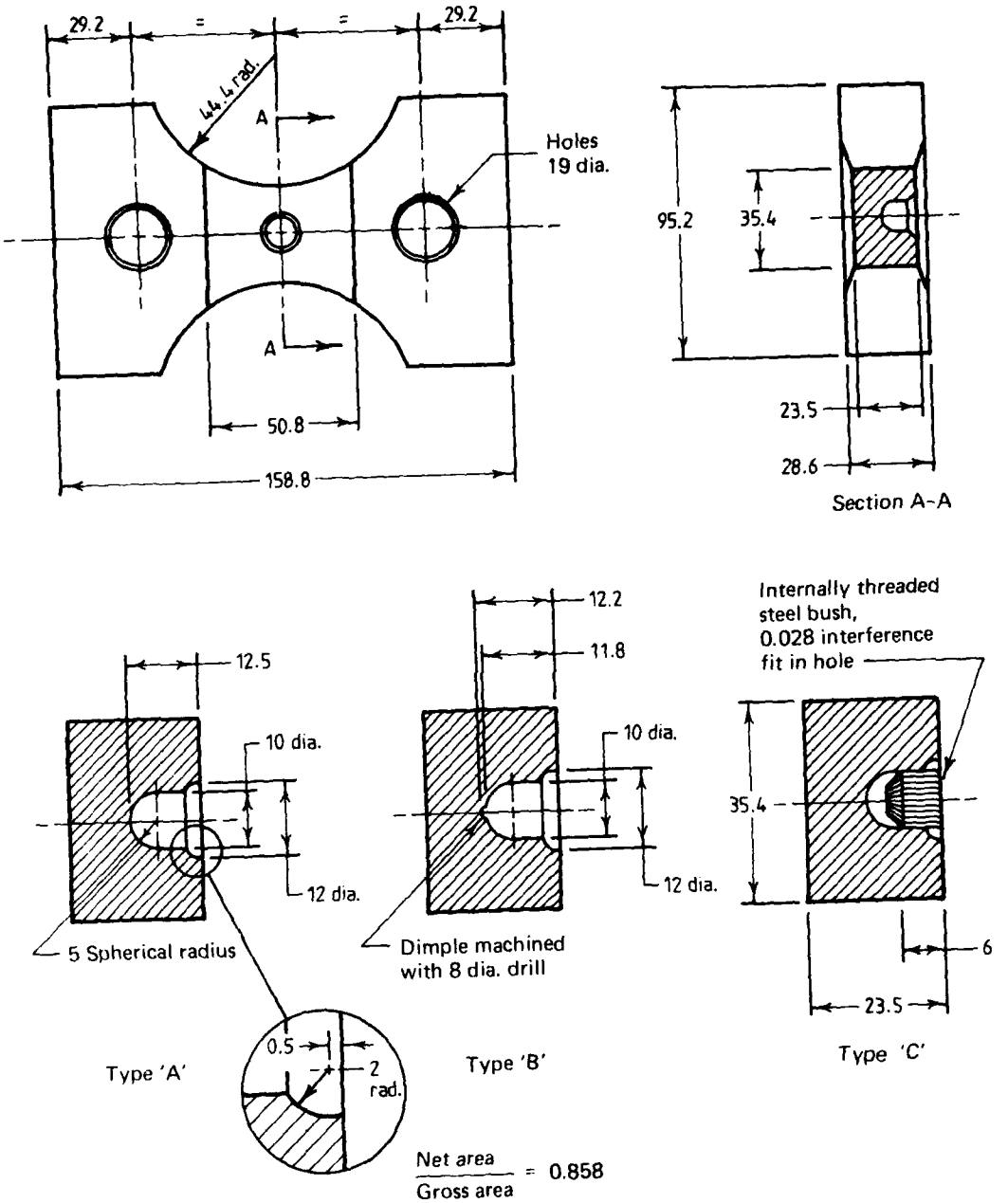

FIG. 5 BLIND ANCHOR-NUT HOLE FATIGUE SPECIMEN

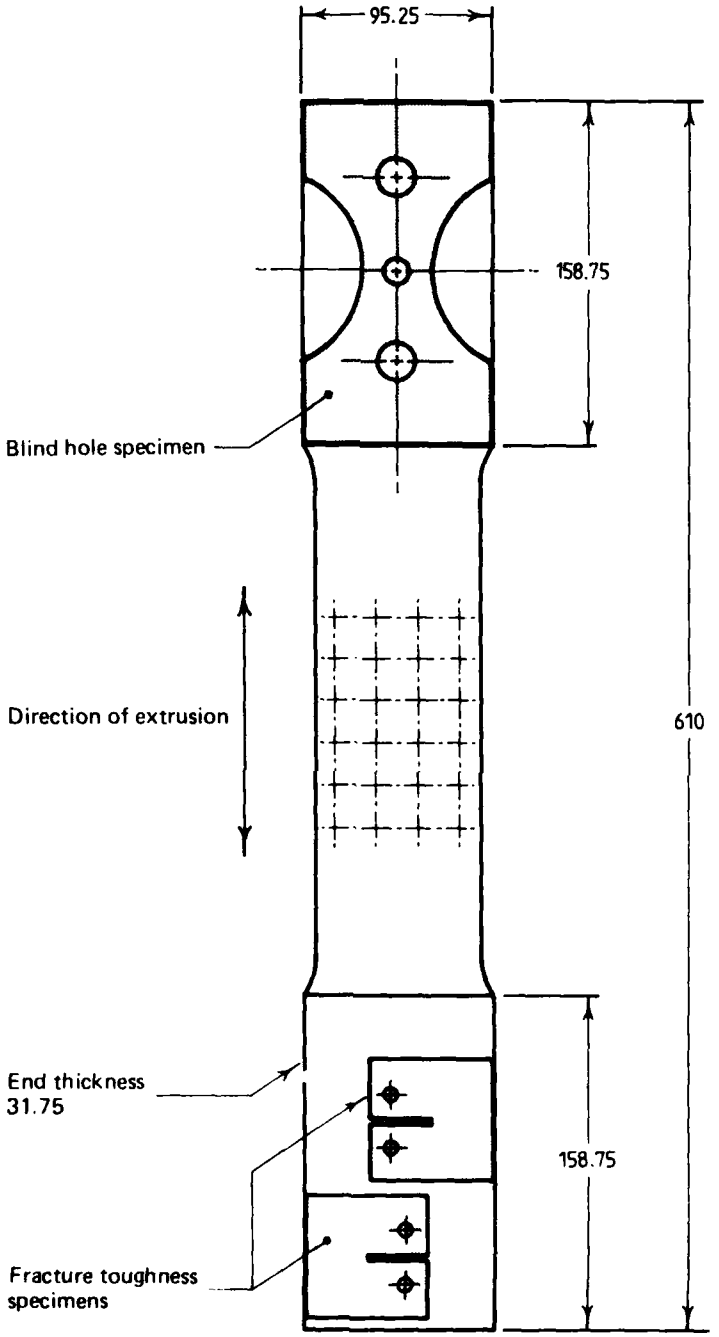

FIG. 6 LOCATION OF SPECIMENS IN LARGER FASTENER SPECIMENS (Ref. 10)

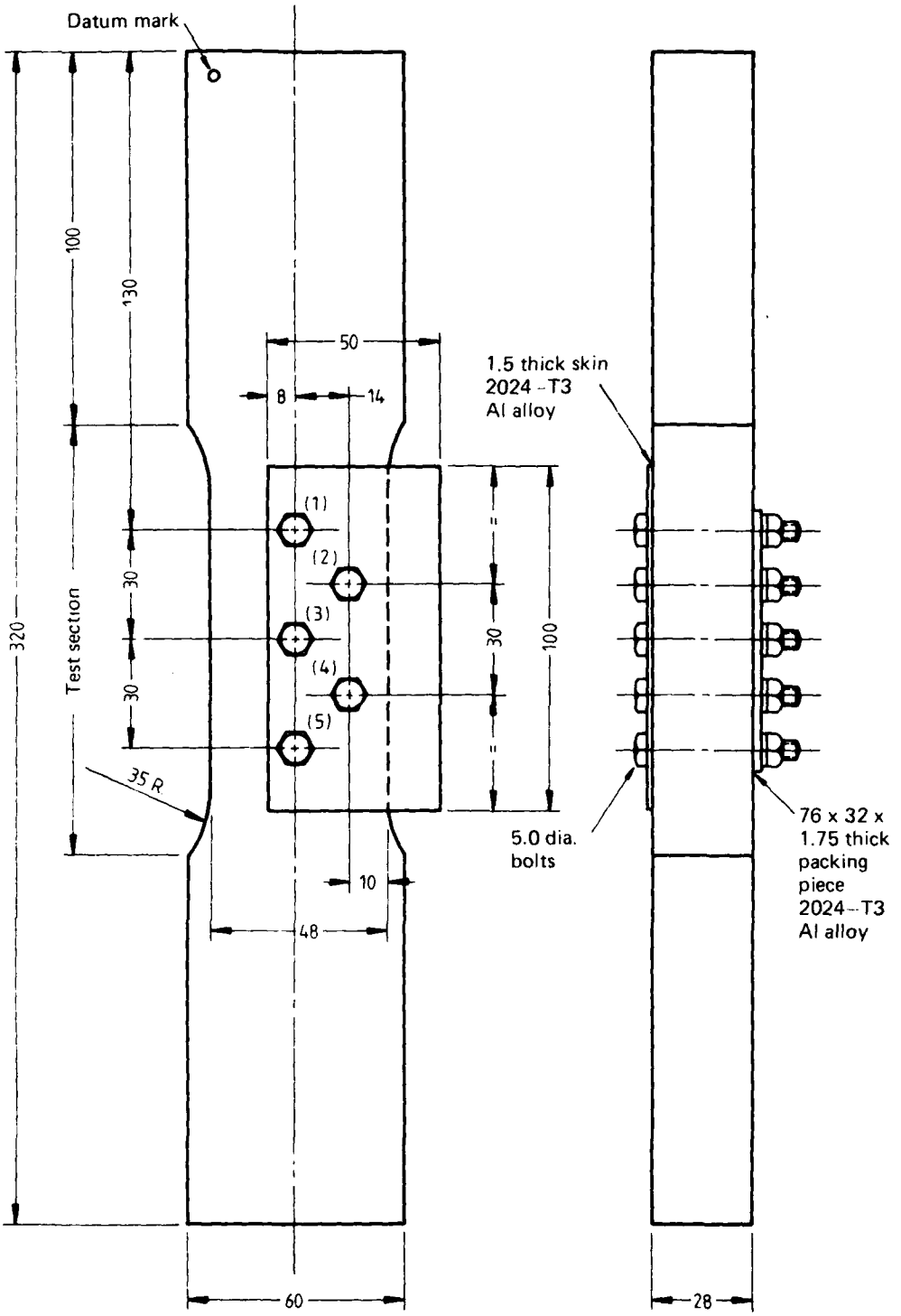

All dimensions in mm
Bolt hole positions in specimen indicated by number in ( )

$\frac{\text{Net area}}{\text{Gross area}} = 0.896$

Material: BS.L168 Al alloy

FIG. 7 FRONT FLANGE BOLT HOLE FATIGUE SPECIMEN

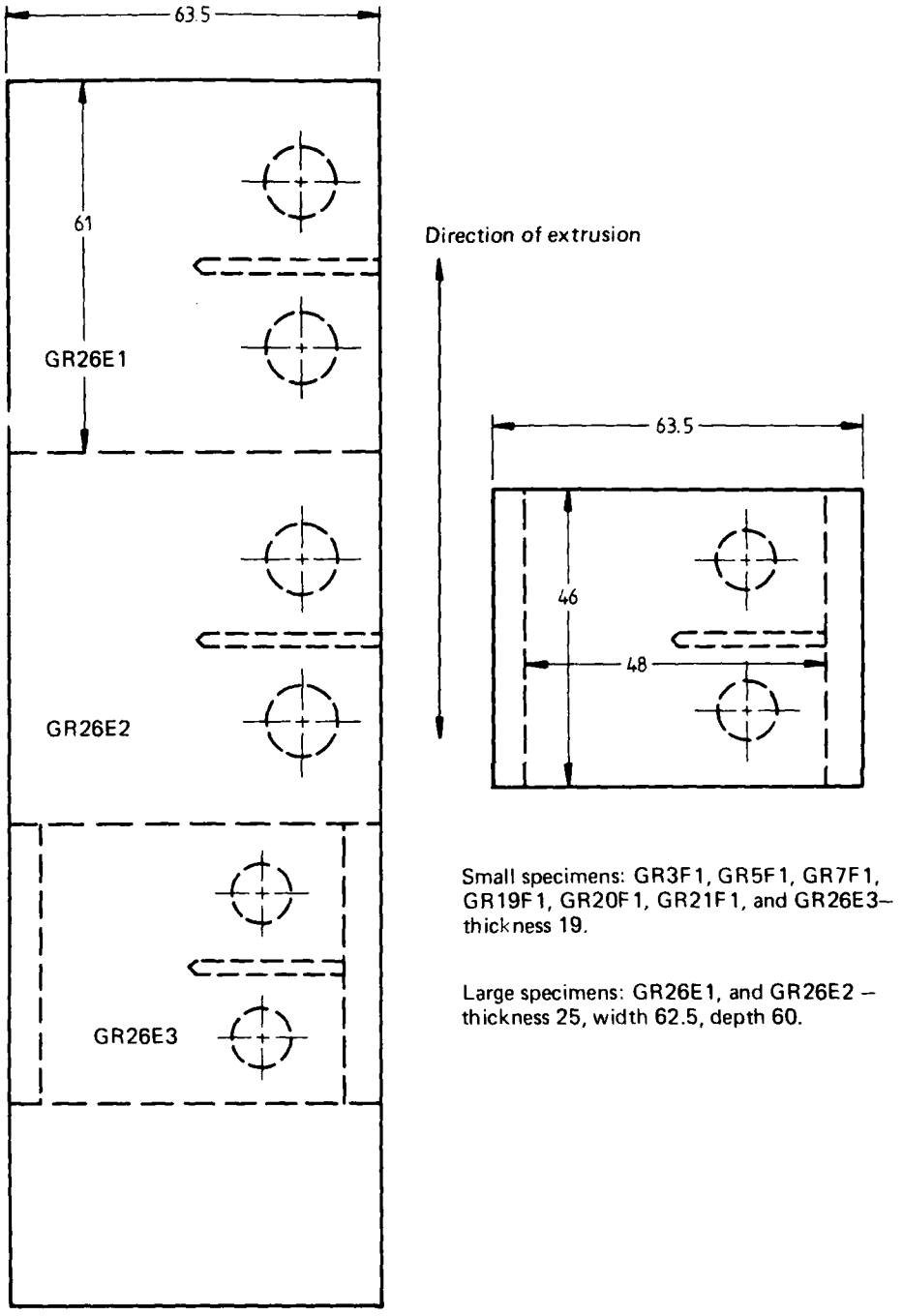

FIG. 8 LOCATIONS OF COMPACT TENSION FRACTURE TOUGHNESS SPECIMENS IN EXTRUDED BARS OF BS.L168 MATERIAL.

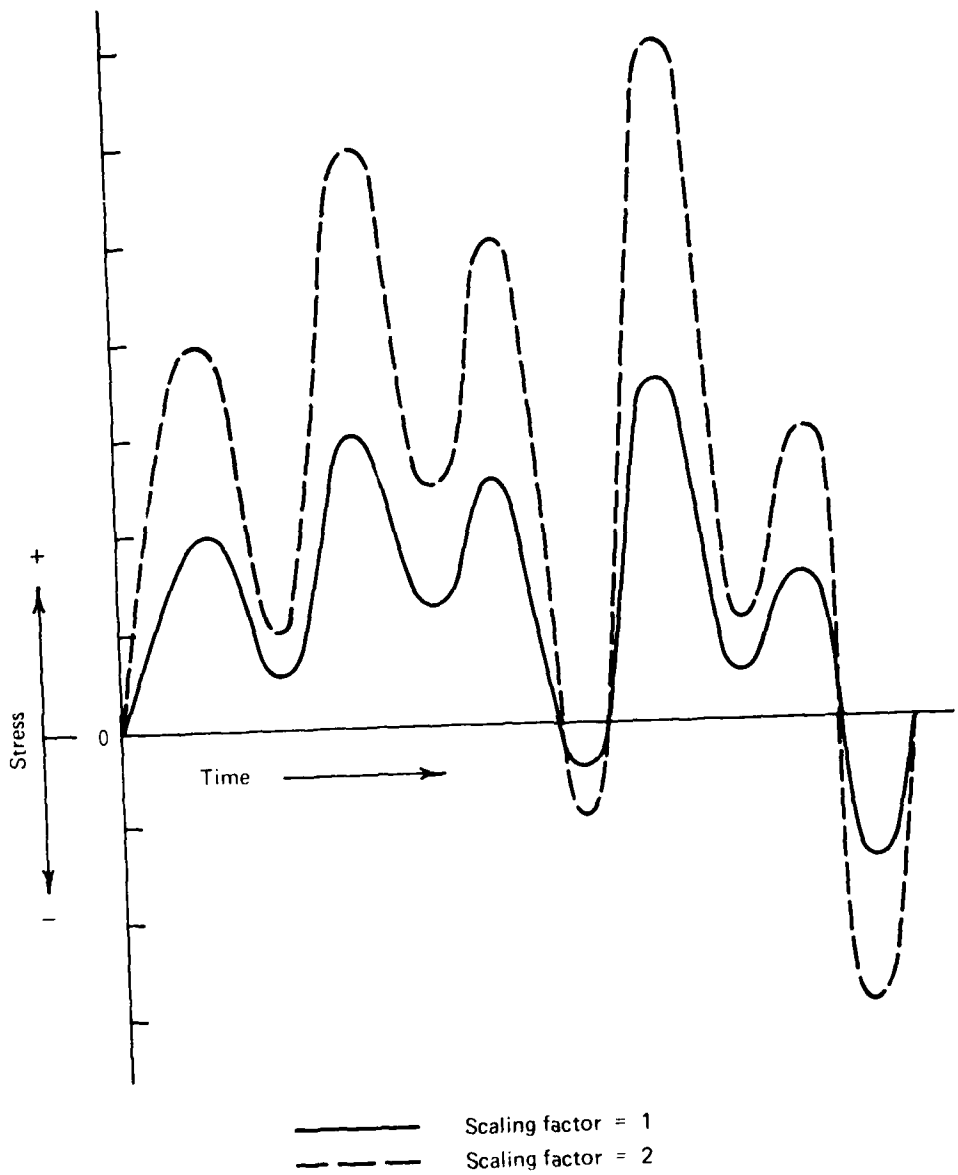

FIG. 9 DEFINITION OF "STRESS SCALING FACTOR"

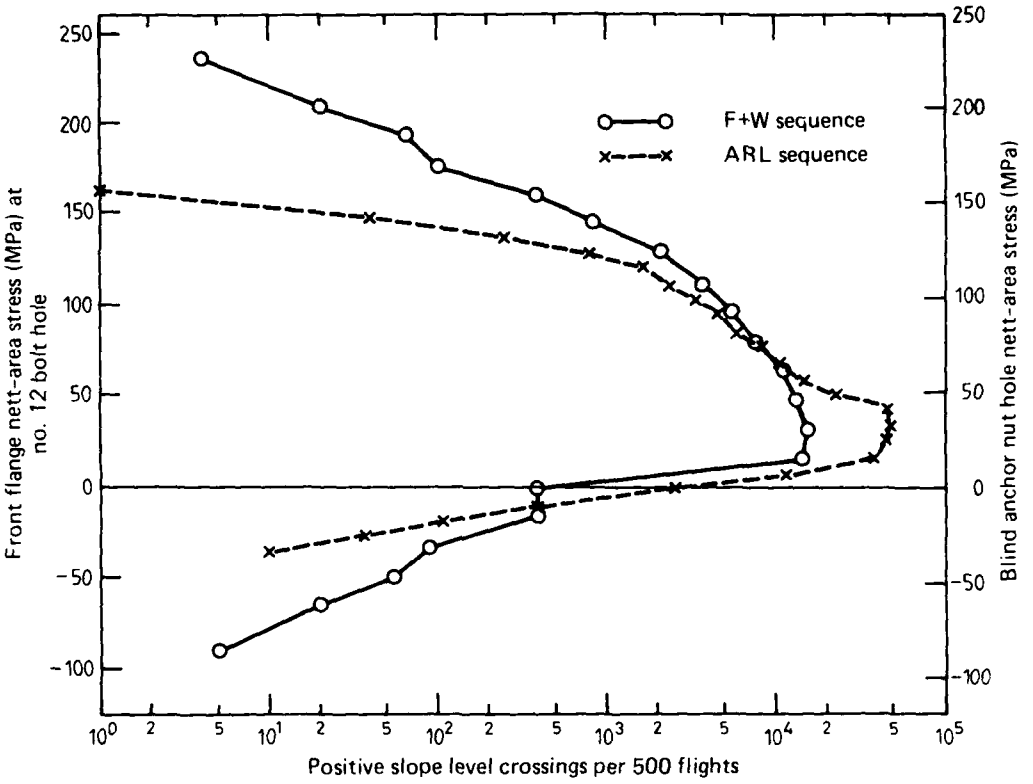

FIG. 10 ARL AND F+W FATIGUE TEST STRESS SPECTRA AT SCALING FACTOR = 1

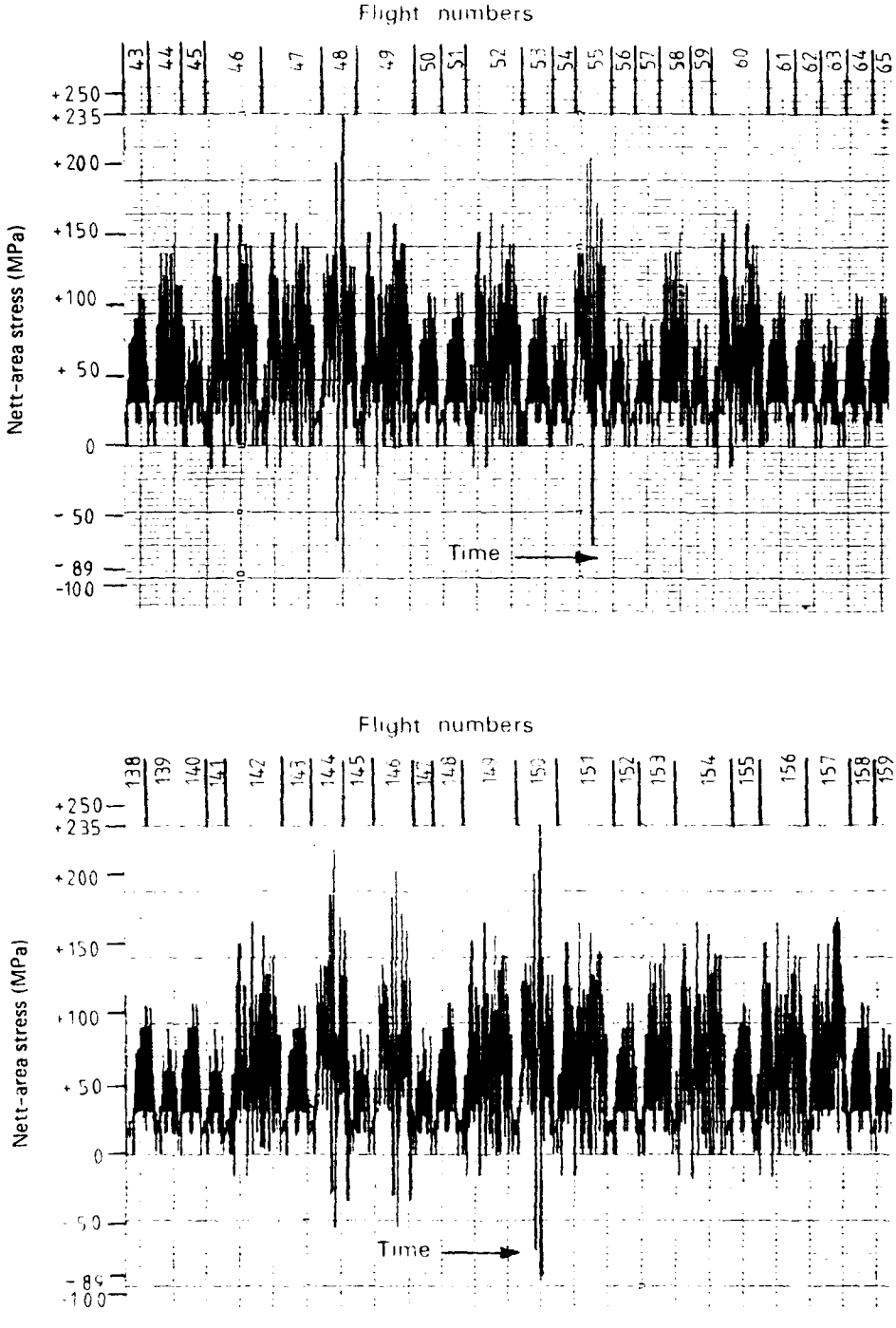

FIG. 11 FRONT FLANGE BOLT HOLE SPECIMENS. STRESS SEQUENCE UNDER THE SWISS SPECTRUM ADJACENT TO FLIGHTS WITH + 7.5 g LOADS. (+ 7.5 g 235 MPa)

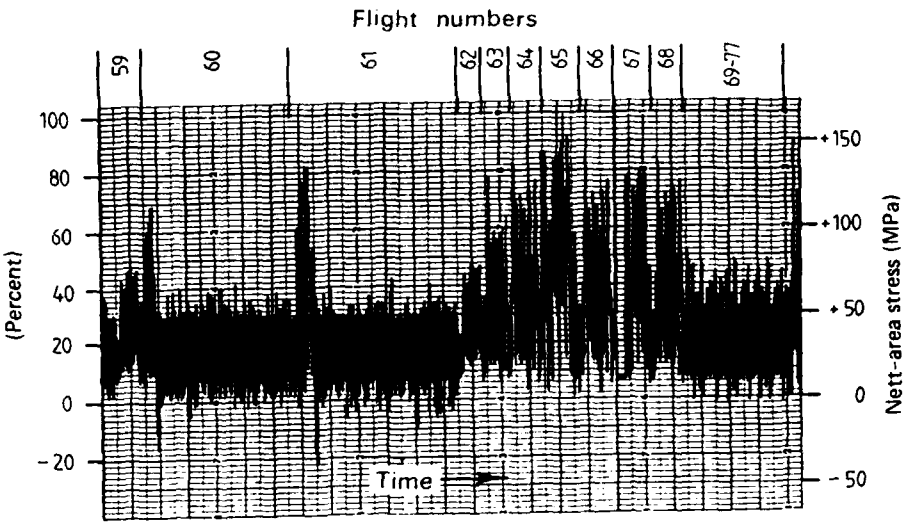

FIG. 12 FRONT FLANGE BOLT HOLE SPECIMENS. STRESS SEQUENCE UNDER THE ARL SPECTRUM INCLUDING THE MAXIMUM (+ 7.8 g IN FLIGHT 65) AND A MINIMUM TURNING POINT (– 1 g IN FLIGHT 61).
+ 7.8 g = 163 MPa

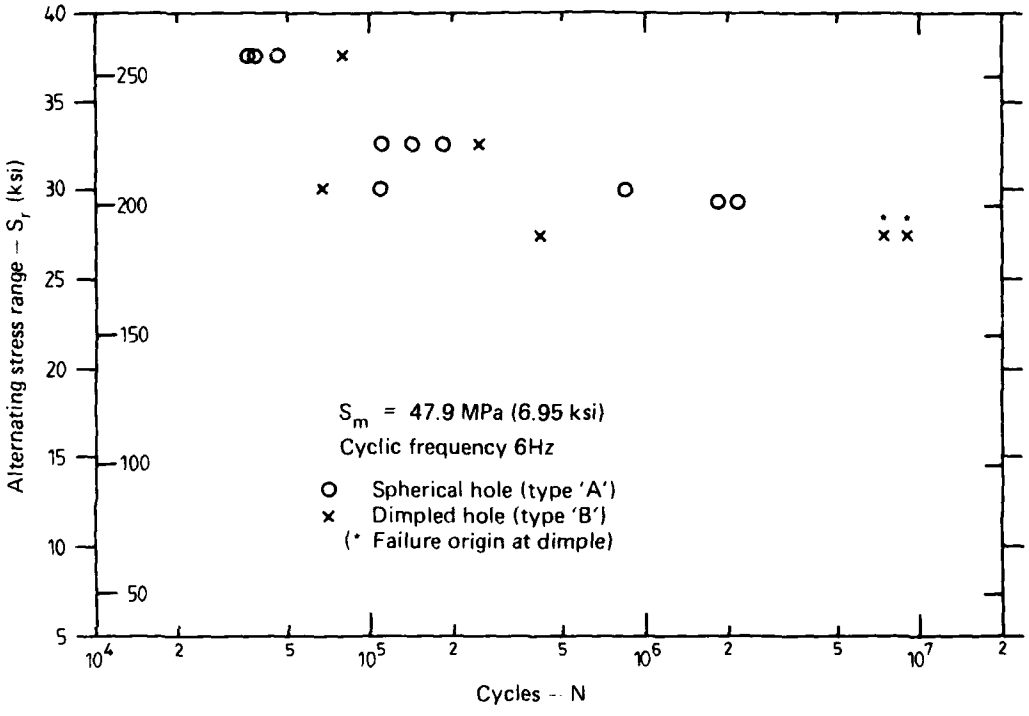

FIG. 13 BLIND-HOLE SPECIMENS – S/N DATA FOR UN-BUSHED HOLES

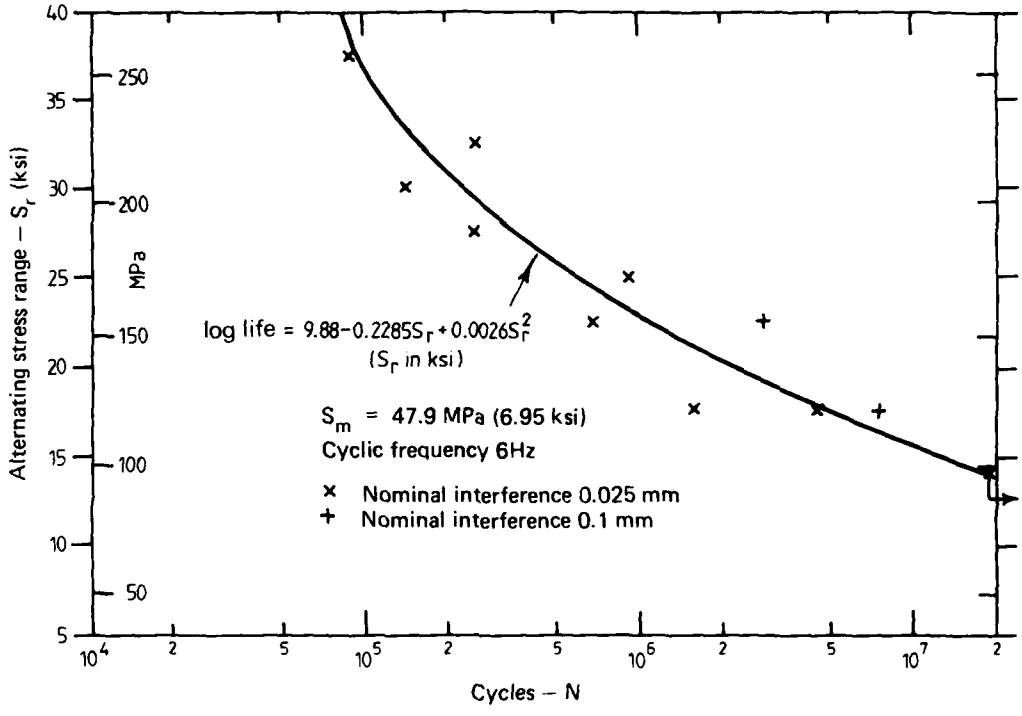

FIG. 14 BLIND-HOLE SPECIMENS – S/N DATA FOR BUSHED DIMPLED HOLES

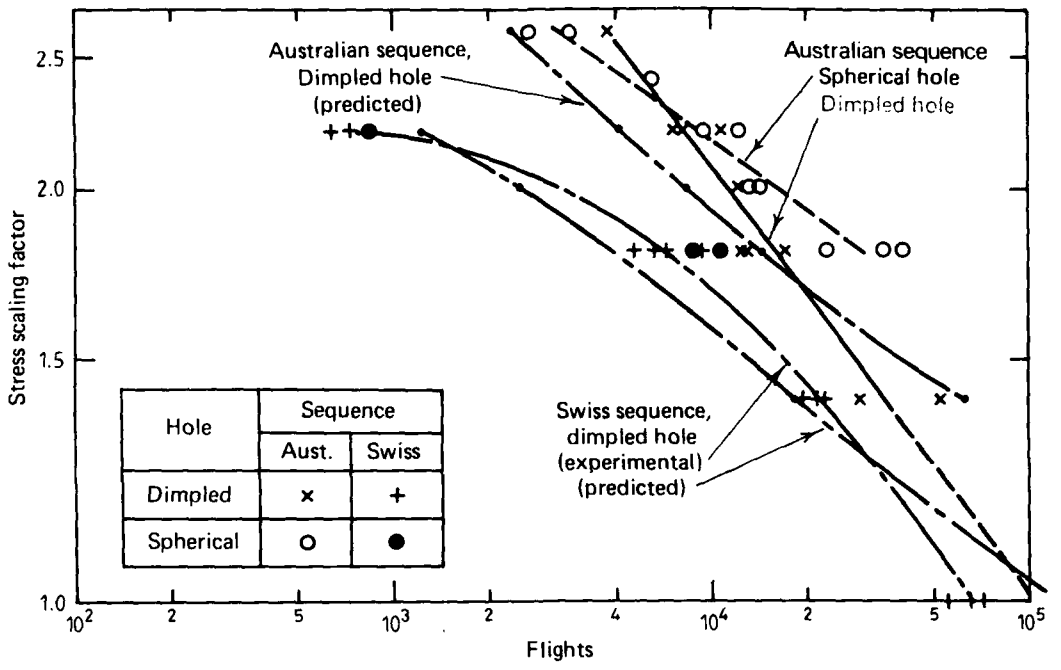

FIG. 15 FATIGUE LIVES OF BUSHED BLIND HOLE SPECIMENS UNDER THE AUSTRALIAN AND SWISS SPECTRA

(a) BJ13D Dimpled hole,
stress scaling factor = 2.2

(b) BJ8H Spherical hole,
stress scaling factor = 1.8

Australian sequence

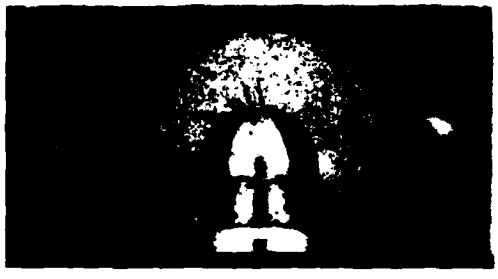

(c) BJ6HB Dimpled hole,
stress scaling factor = 1.8

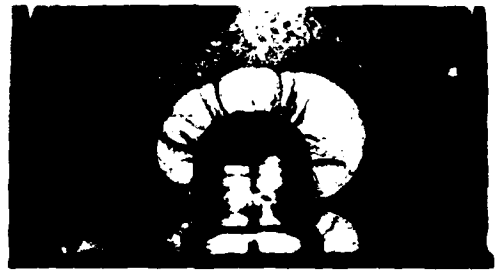

(d) BJ12F Spherical hole
stress scaling factor = 1.8

Swiss sequence

FIG. 16 FRACTURE SURFACES, BLIND HOLE (BUSHED) SPECIMENS

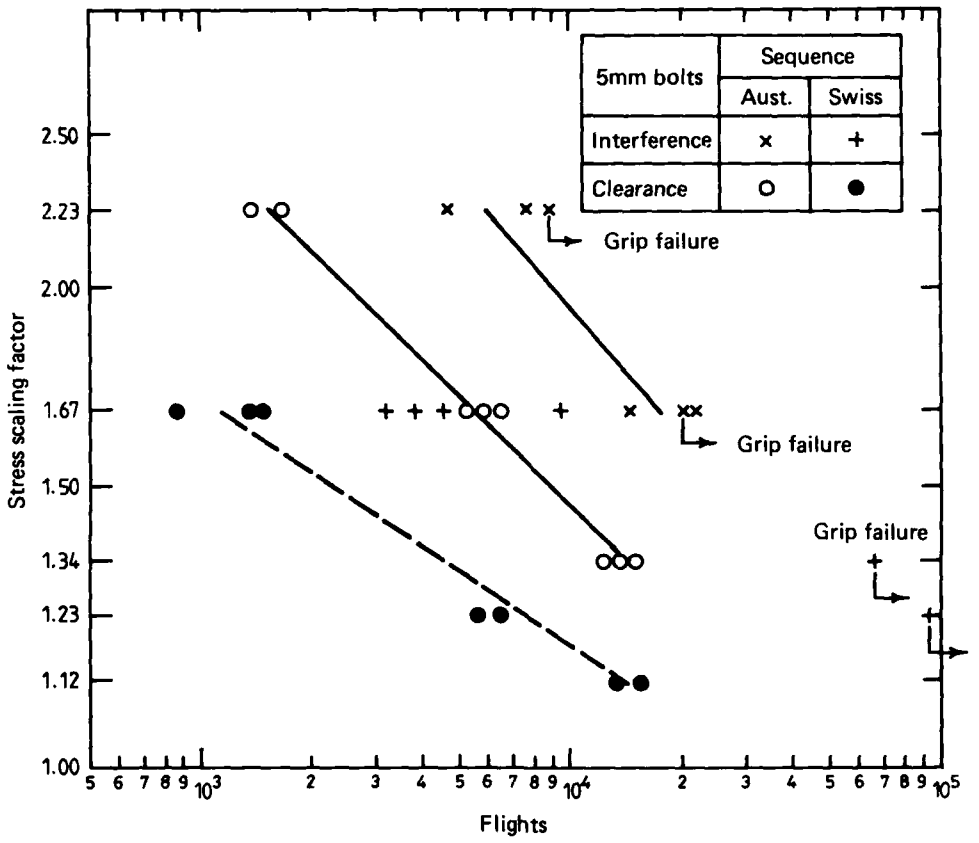

FIG. 17 FRONT FLANGE SPECIMENS – TESTS UNDER AUSTRALIAN AND SWISS SEQUENCES

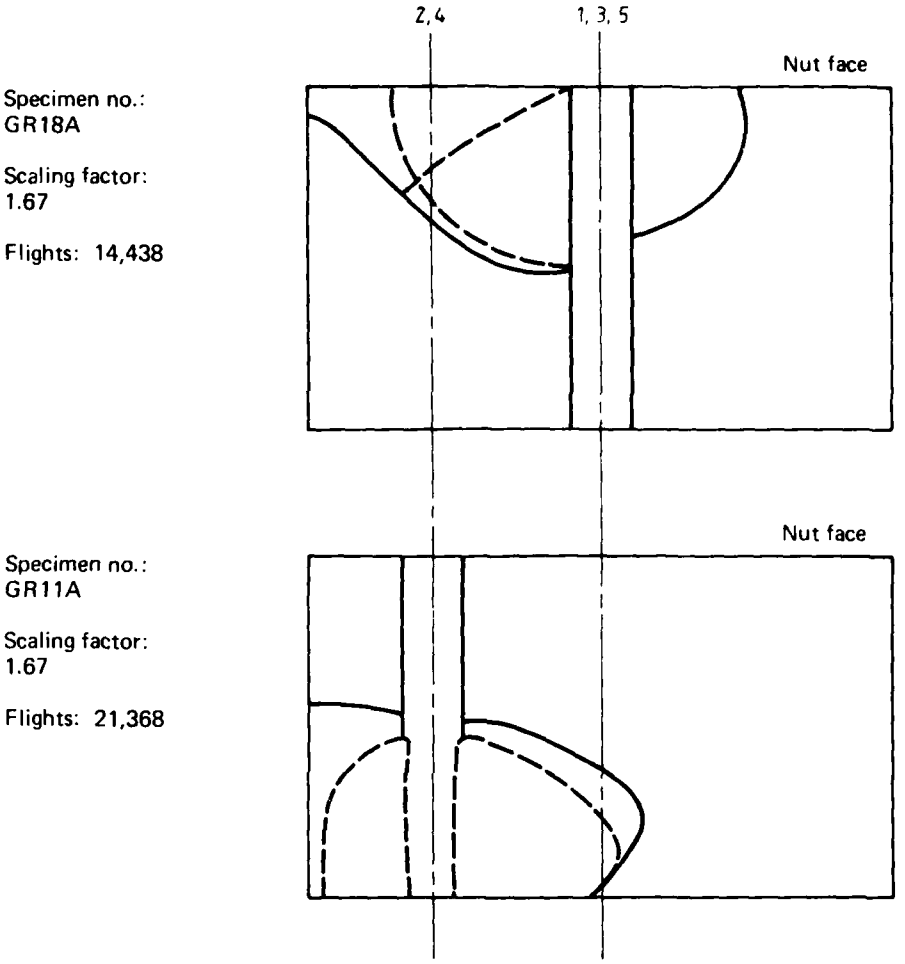

FIG. 18 (a) FRACTURE SURFACES, FRONT FLANGE SPECIMENS, AUSTRALIAN SEQUENCE, INTERFERENCE-FIT BOLTS

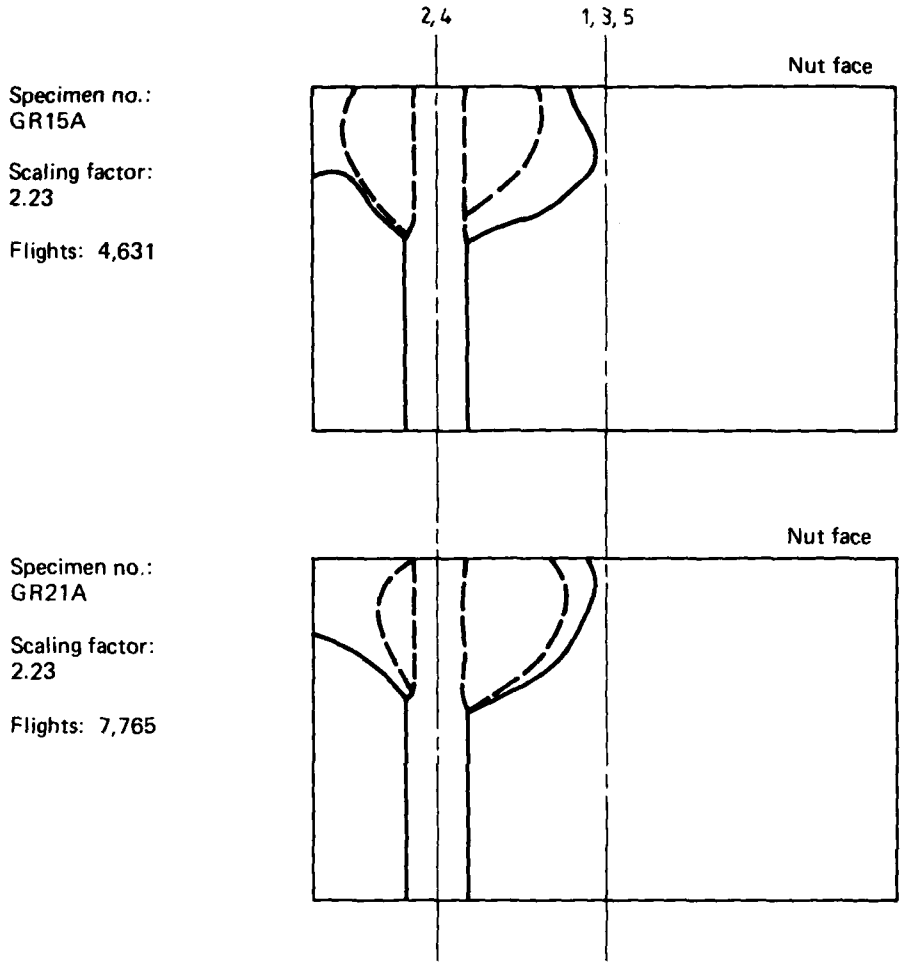

(The full lines indicate the approximate extent of fatigue cracking before final failure, while the dashed lines represent the approximate boundaries of the 'flat' area of the major crack before the development of shear lips at an advanced stage of the crack propagation. The dot-dash lines represent the approximate boundaries of the shear lips at final fracture.)

FIG. 18(a) FRACTURE SURFACES, FRONT FLANGE SPECIMENS, AUSTRALIAN SEQUENCE, INTERFERENCE-FIT BOLTS

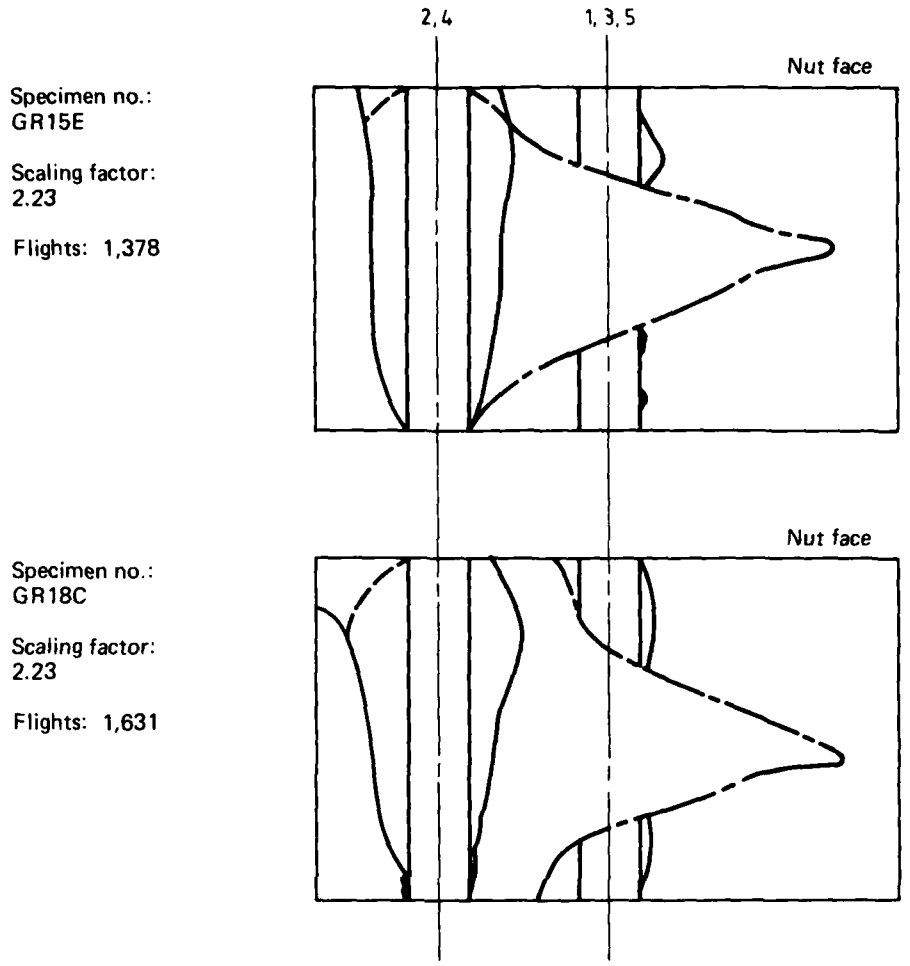

FIG. 18(b) *FRACTURE SURFACES, FRONT FLANGE SPECIMENS, AUSTRALIAN SEQUENCE, CLEARANCE-FIT BOLTS*

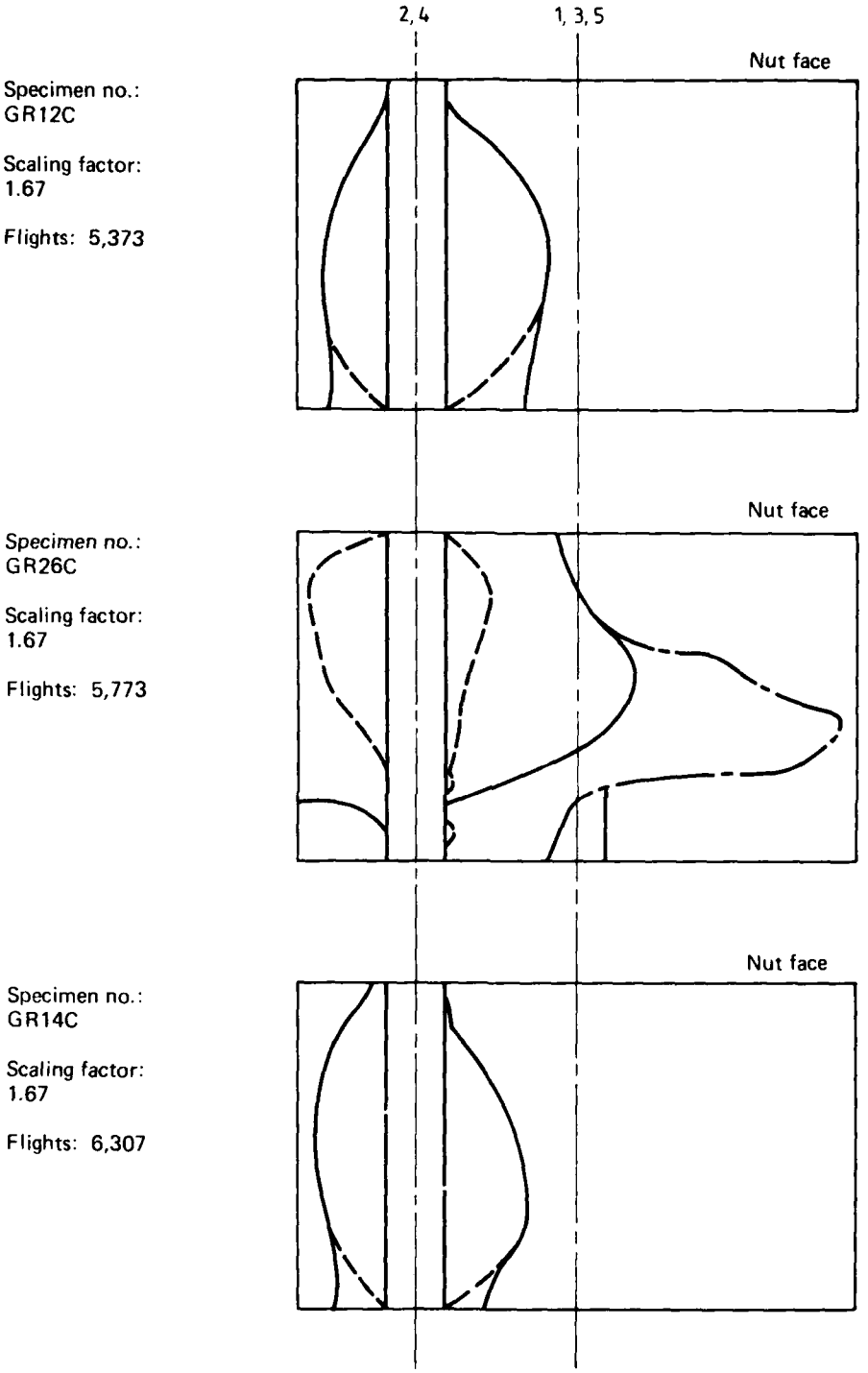

FIG. 18(b) FRACTURE SURFACES, FRONT FLANGE SPECIMENS, AUSTRALIAN SEQUENCE, CLEARANCE-FIT BOLTS

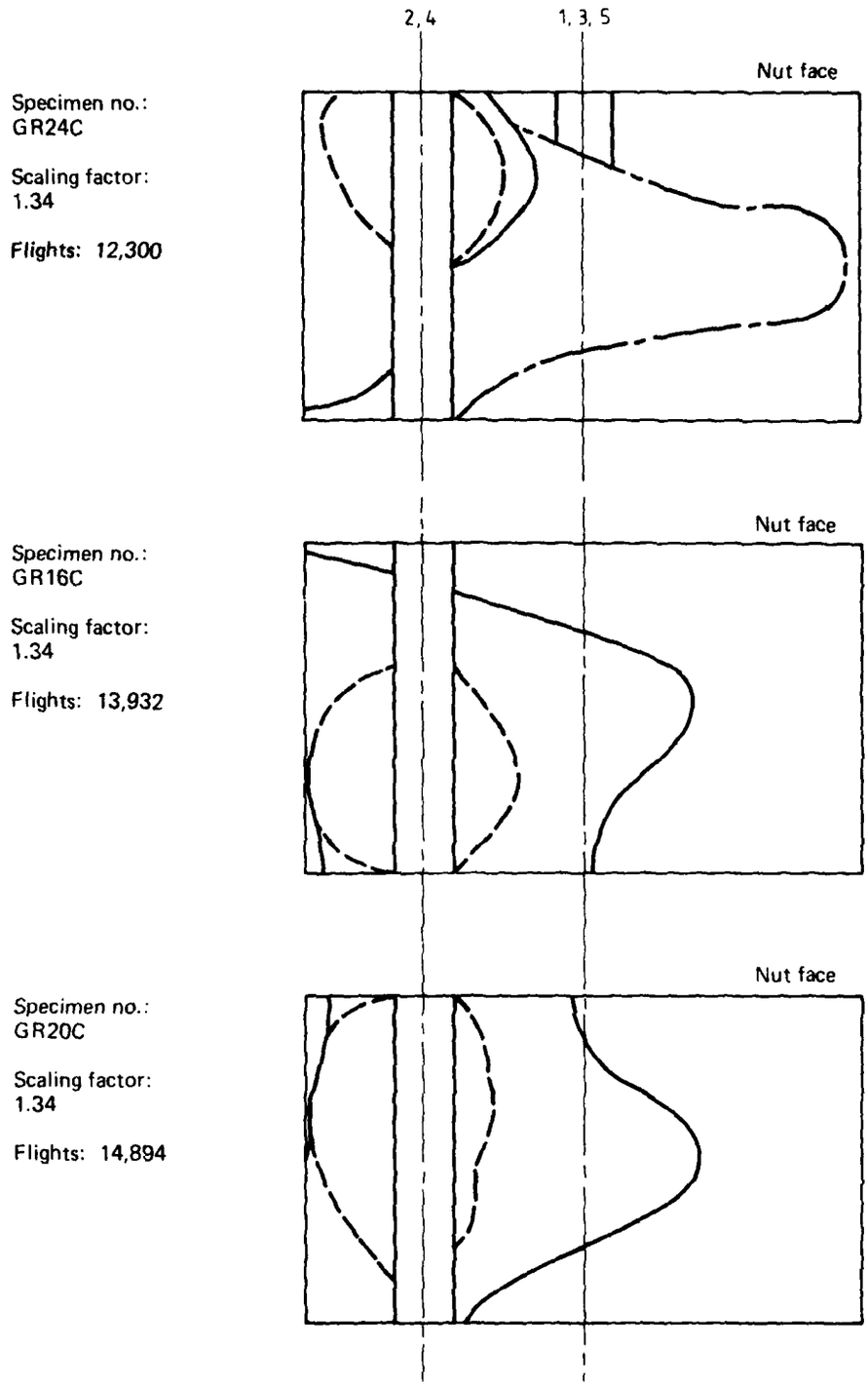

FIG. 18(b) FRACTURE SURFACES, FRONT FLANGE SPECIMENS, AUSTRALIAN SEQUENCE, CLEARANCE-FIT BOLTS

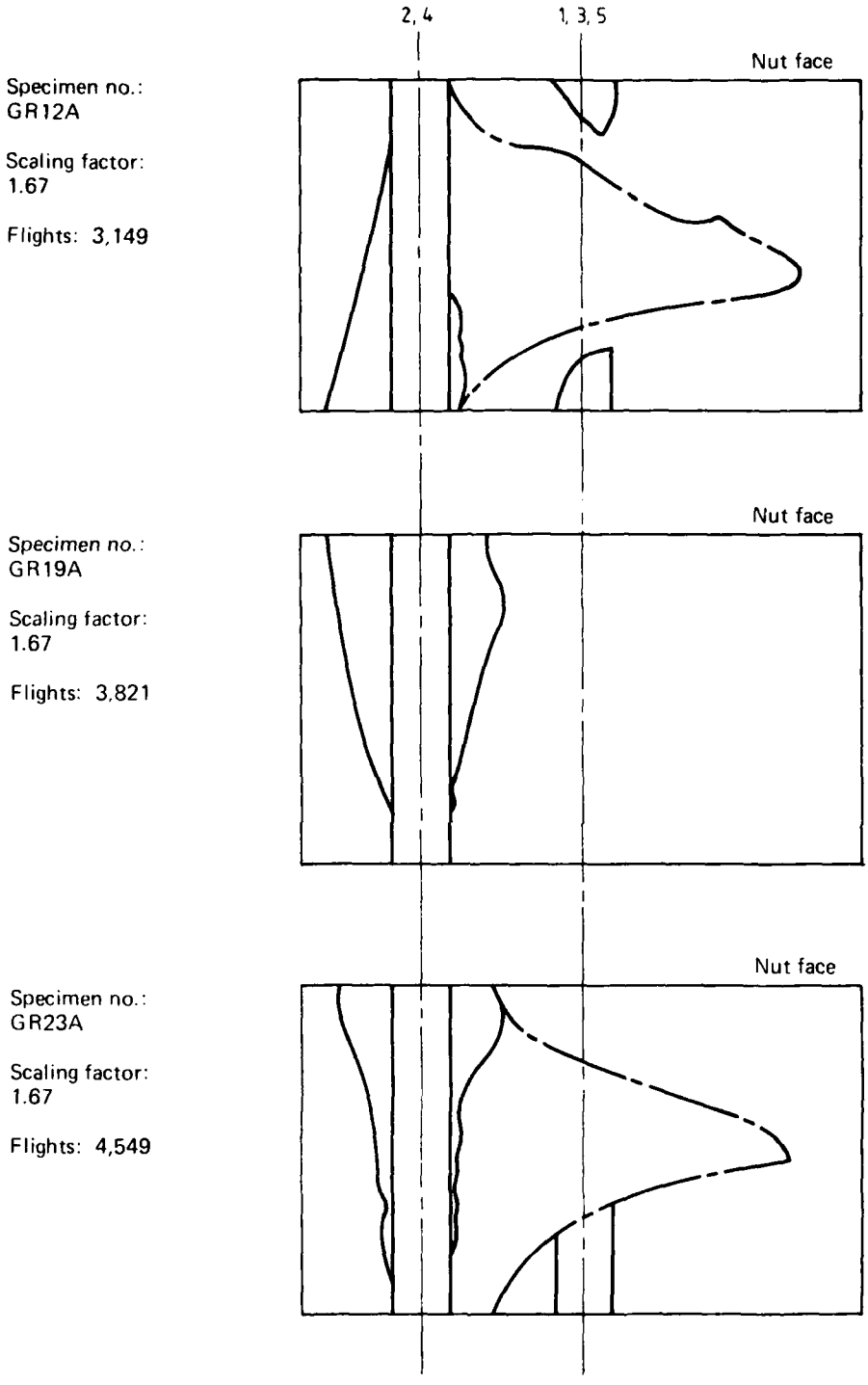

FIG. 18(c) FRACTURE SURFACES, FRONT FLANGE SPECIMENS, SWISS SEQUENCE, INTERFERENCE-FIT BOLTS

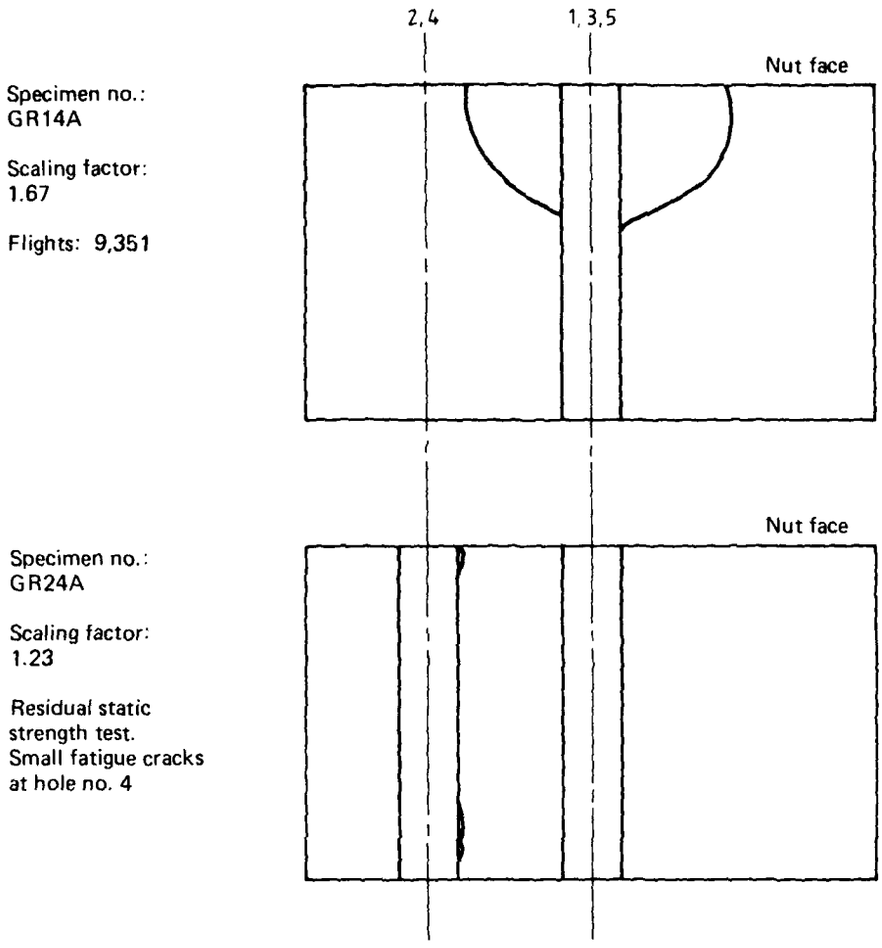

FIG. 18(c) FRACTURE SURFACES, FRONT FLANGE SPECIMENS, SWISS SEQUENCE, INTERFERENCE-FIT BOLTS

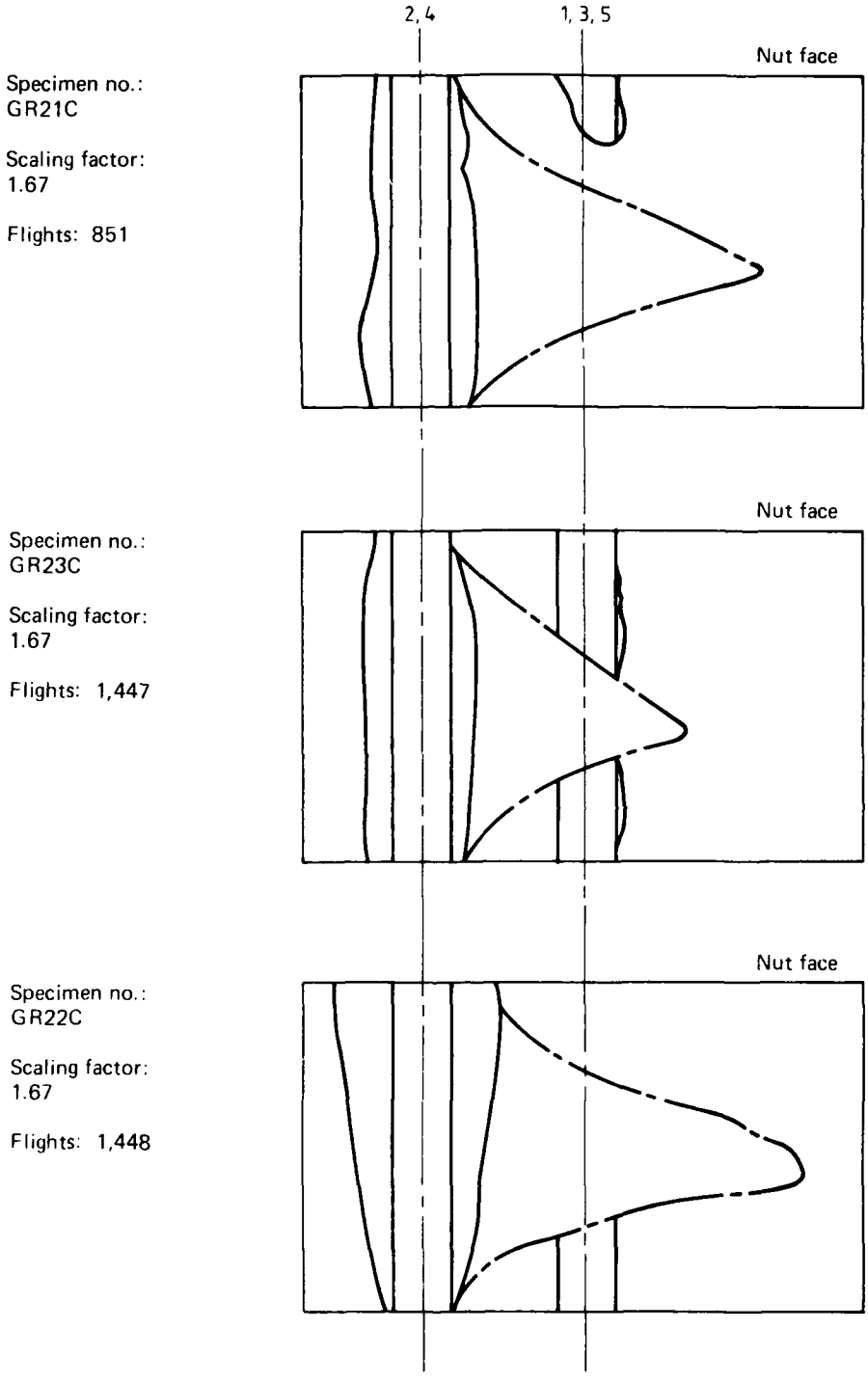

FIG. 18(d) FRACTURE SURFACES, FRONT FLANGE SPECIMENS, SWISS SEQUENCE, CLEARANCE-FIT BOLTS

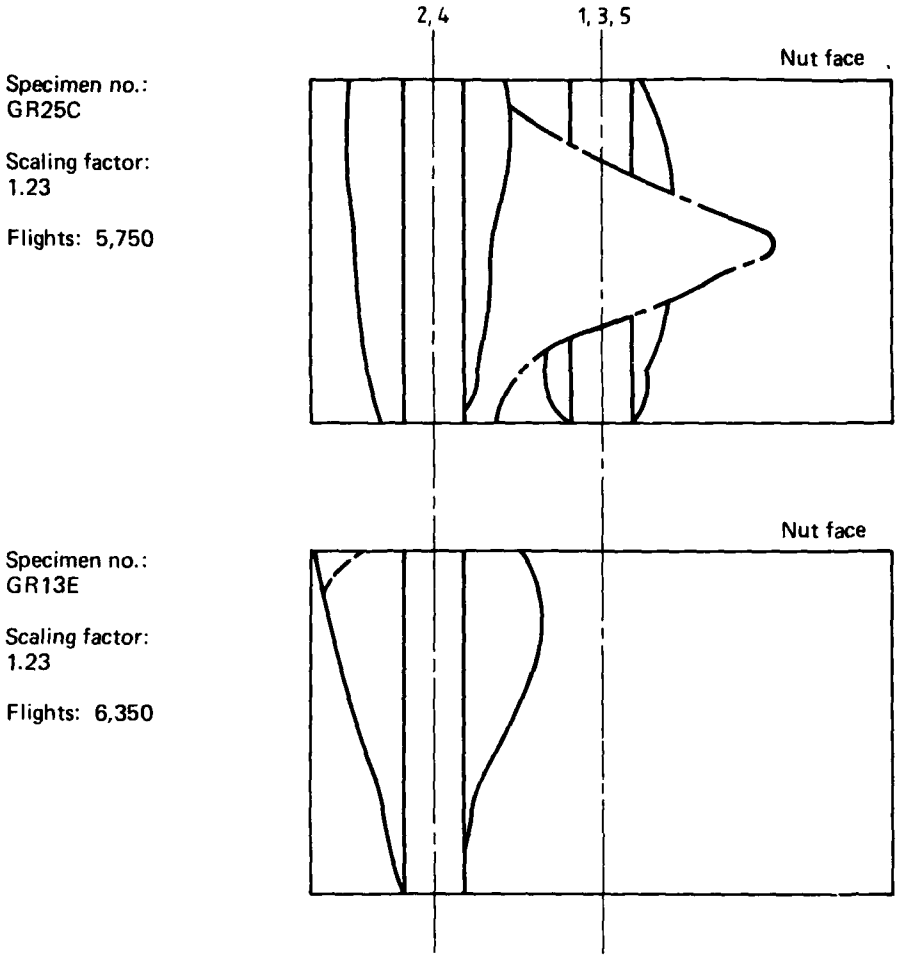

FIG. 18(d) FRACTURE SURFACES, FRONT FLANGE SPECIMENS, SWISS SEQUENCE, CLEARANCE-FIT BOLTS

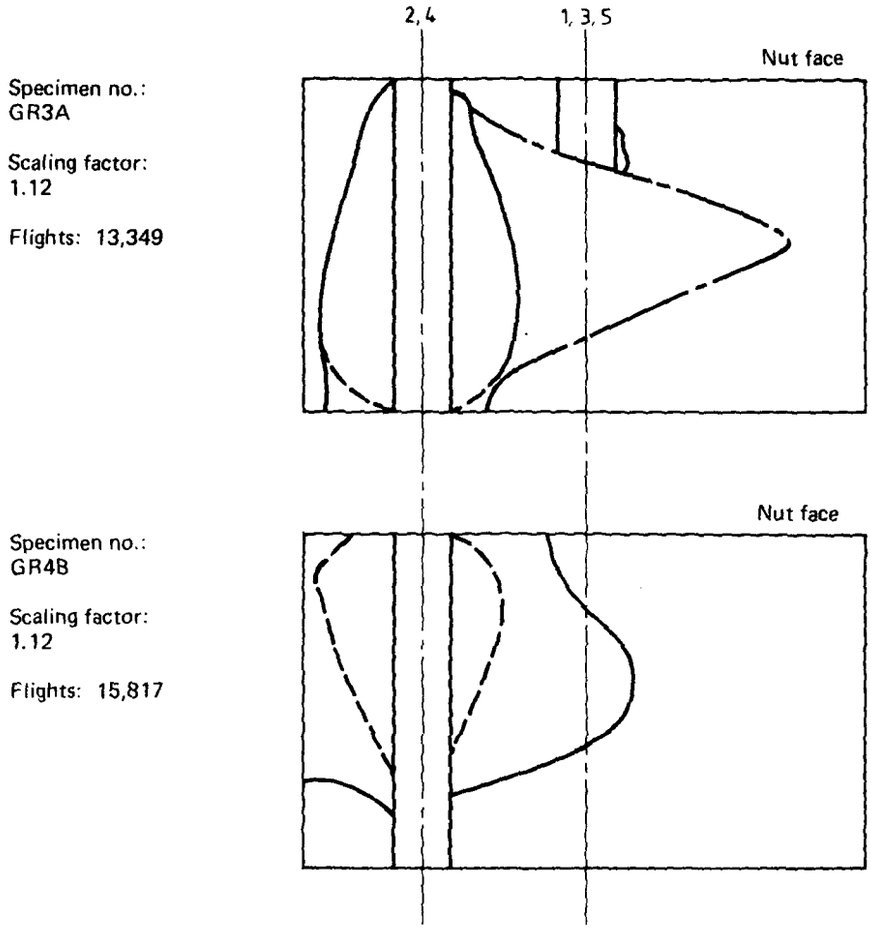

FIG. 18(d) FRACTURE SURFACES, FRONT FLANGE SPECIMENS, SWISS SEQUENCE, CLEARANCE-FIT BOLTS

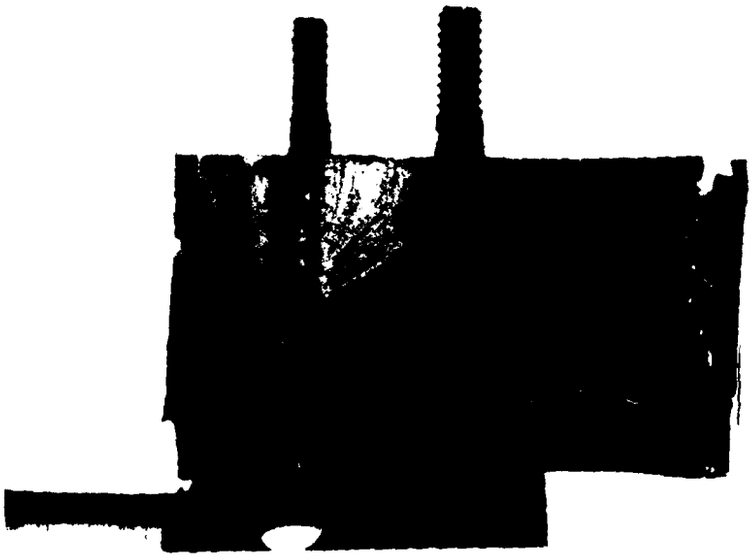

(i) GR21A, interference-fit bolts

(ii) GR14C, clearance-fit bolts

FIG. 19(a) FRACTURE SURFACES, FRONT FLANGE SPECIMENS, AUSTRALIAN SEQUENCE

(i) GR14A, interference-fit bolts

(ii) GR25C, clearance-fit bolts

FIG. 19(b) FRACTURE SURFACES, FRONT FLANGE SPECIMENS, SWISS SEQUENCE

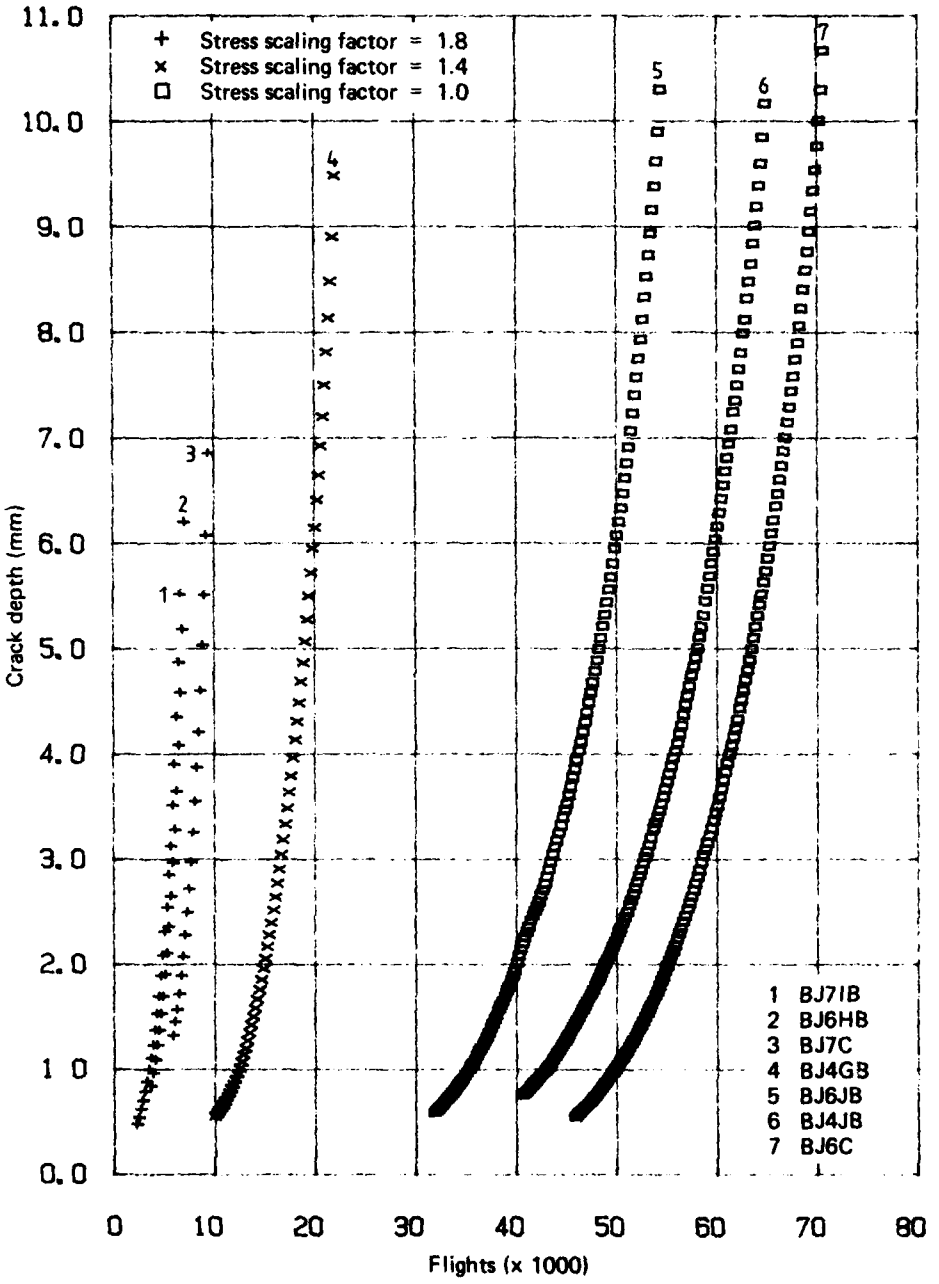

FIG. 20(a) BLIND-HOLE SPECIMENS, FATIGUE CRACK PROPAGATION UNDER THE SWISS SEQUENCE

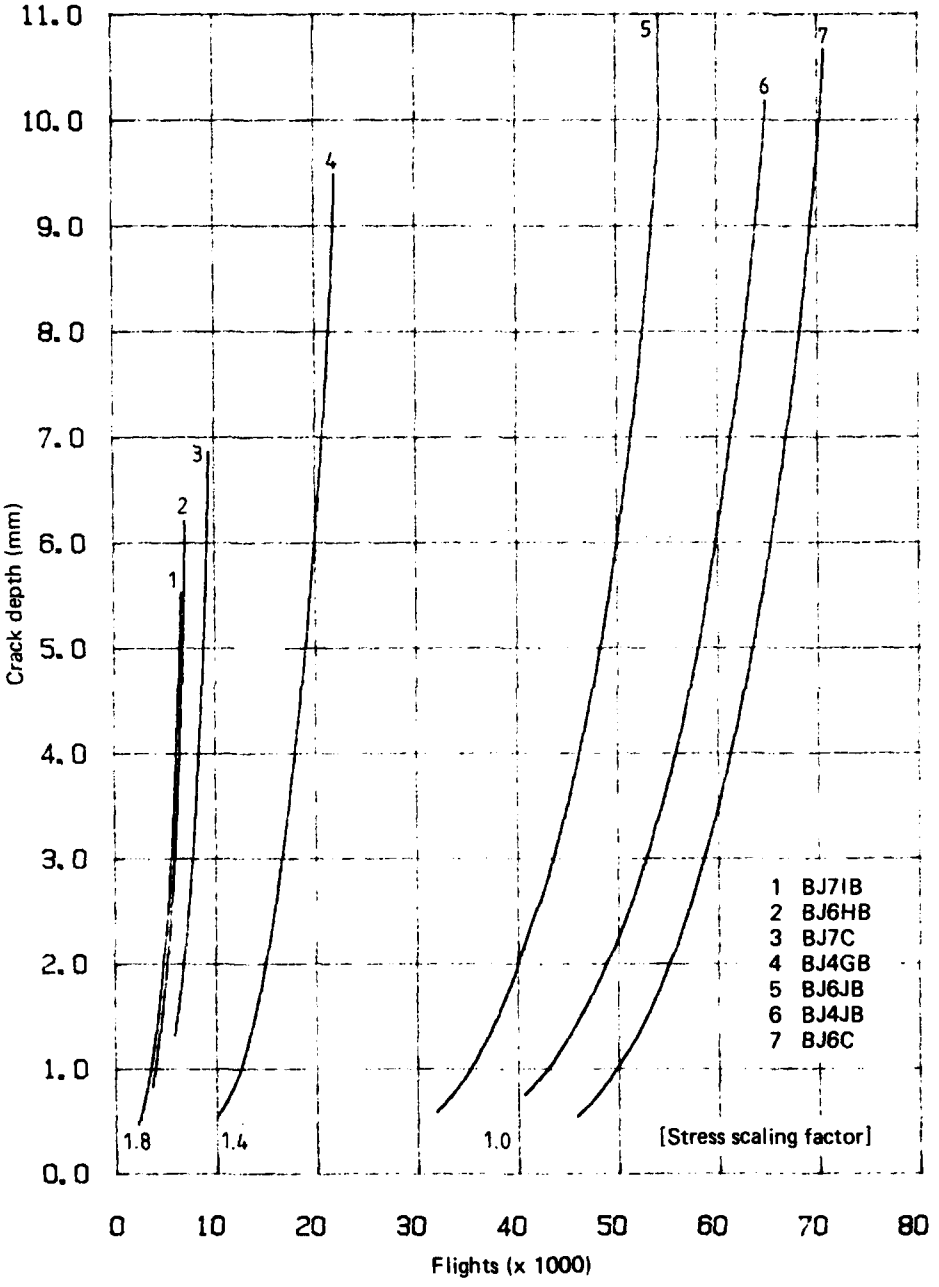

FIG. 20(b) BLIND HOLE SPECIMENS, FATIGUE CRACK PROPAGATION UNDER THE SWISS SEQUENCE

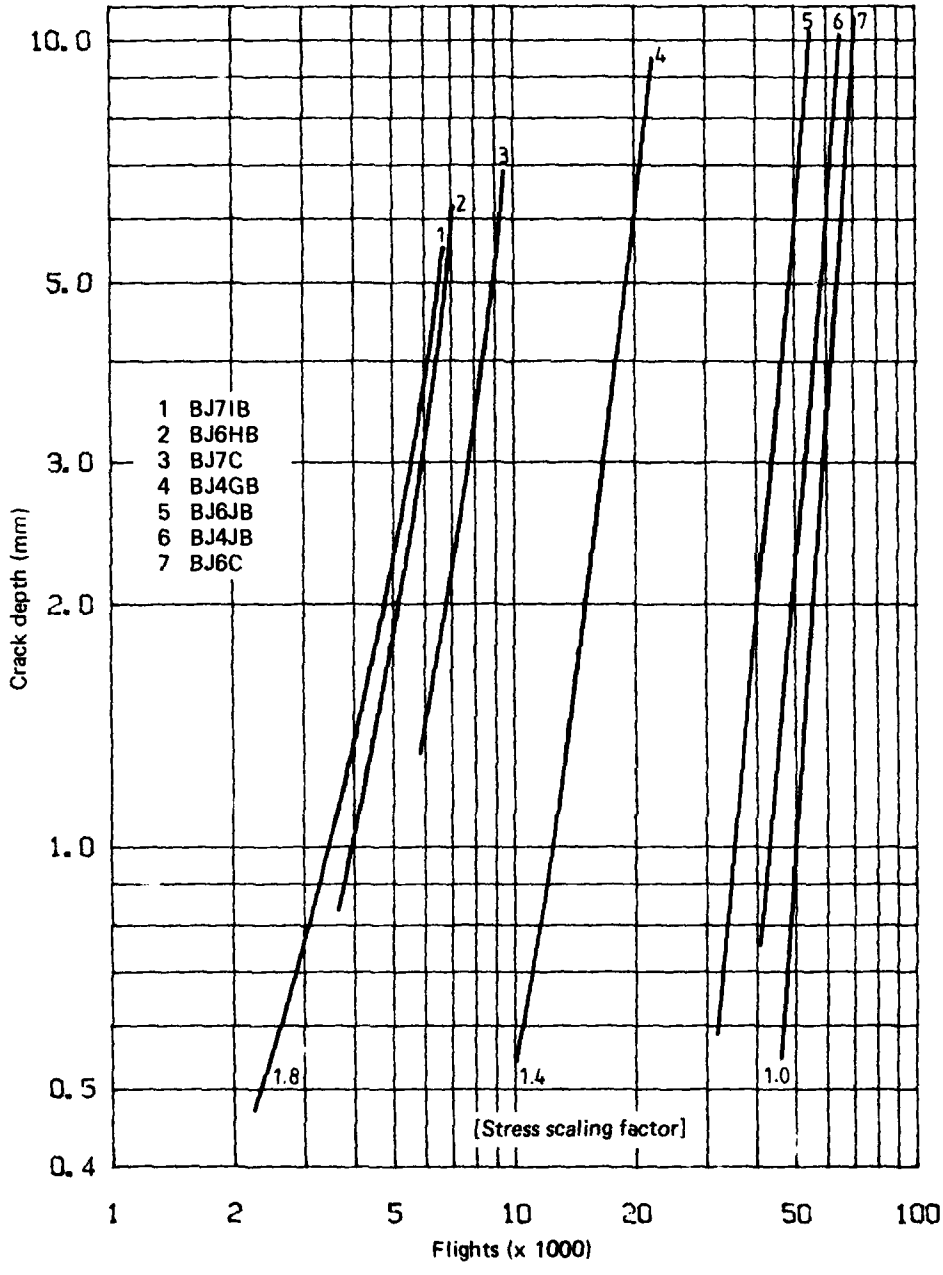

FIG. 20(c) BLIND HOLE SPECIMENS, FATIGUE CRACK PROPAGATION UNDER THE SWISS SEQUENCE

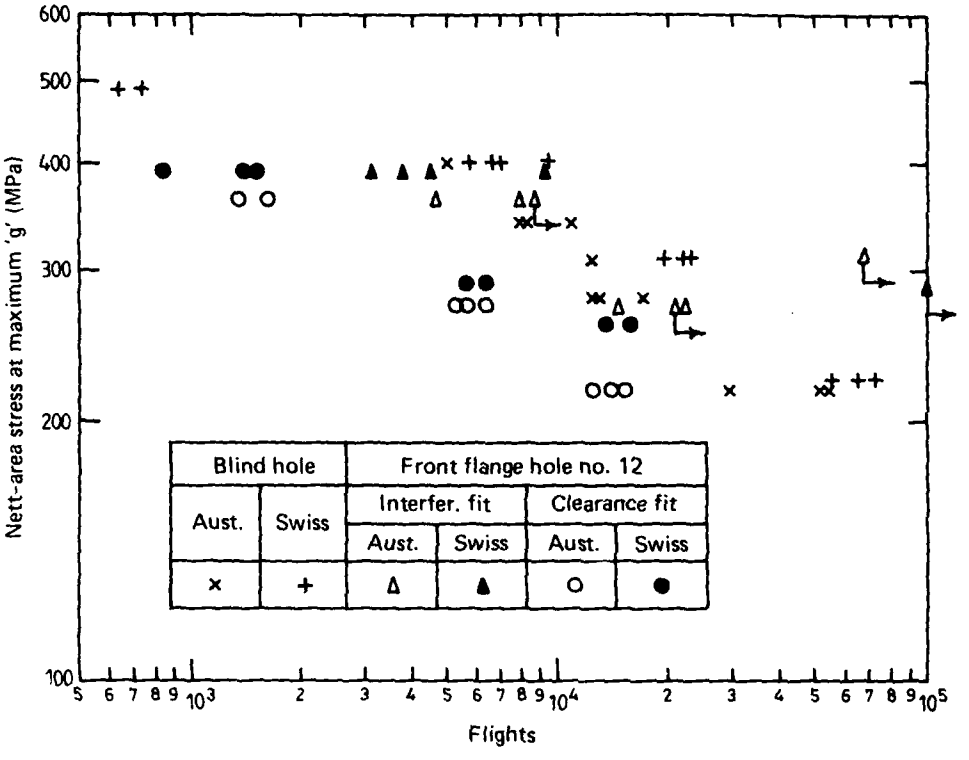

FIG. 21 COMPARISON OF FATIGUE LIVES BASED ON STRESSES AT MAXIMUM 'g' FOR DIFFERENT SCALING FACTORS

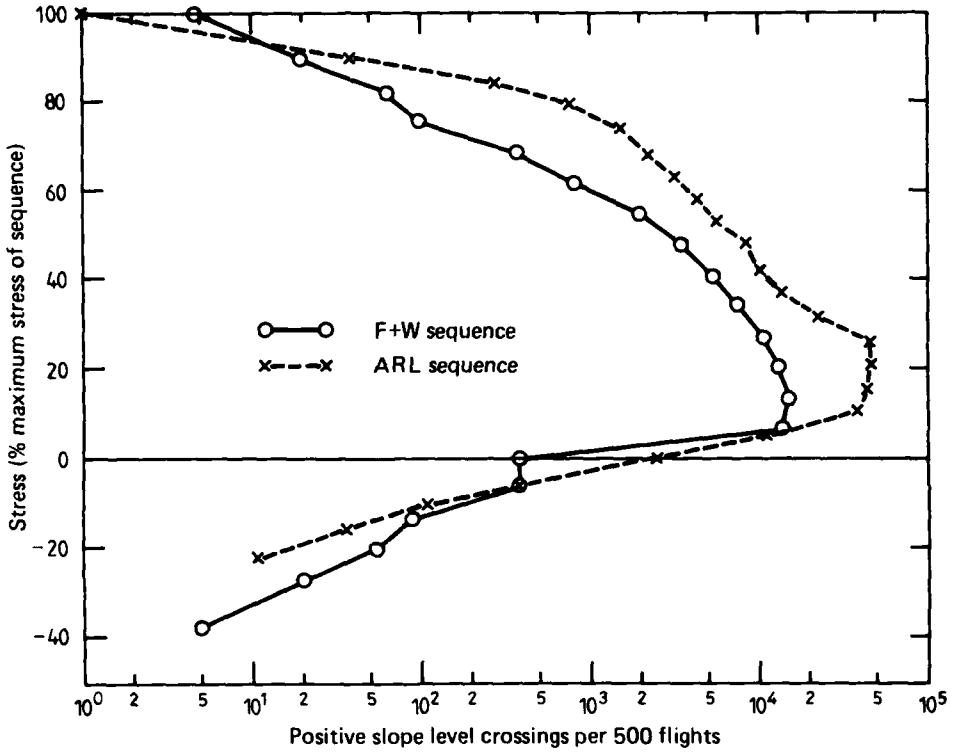

FIG. 22 EXCEEDANCES VERSUS NORMALISED STRESSES FOR ARL AND F+W TEST SPECTRA

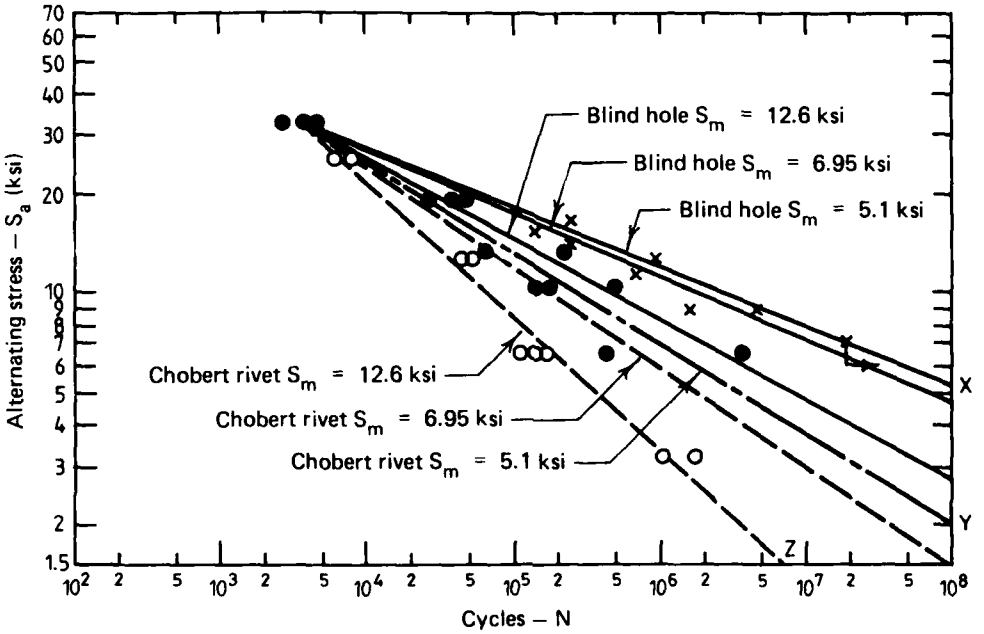

× Blind hole S_m = 6.95 ksi
○ Chobert rivet S_m = 12.6 ksi
● Chobert rivet S_m = 5.1 ksi

FIG. 23 BASIC S/N DATA FOR LIFE ESTIMATIONS

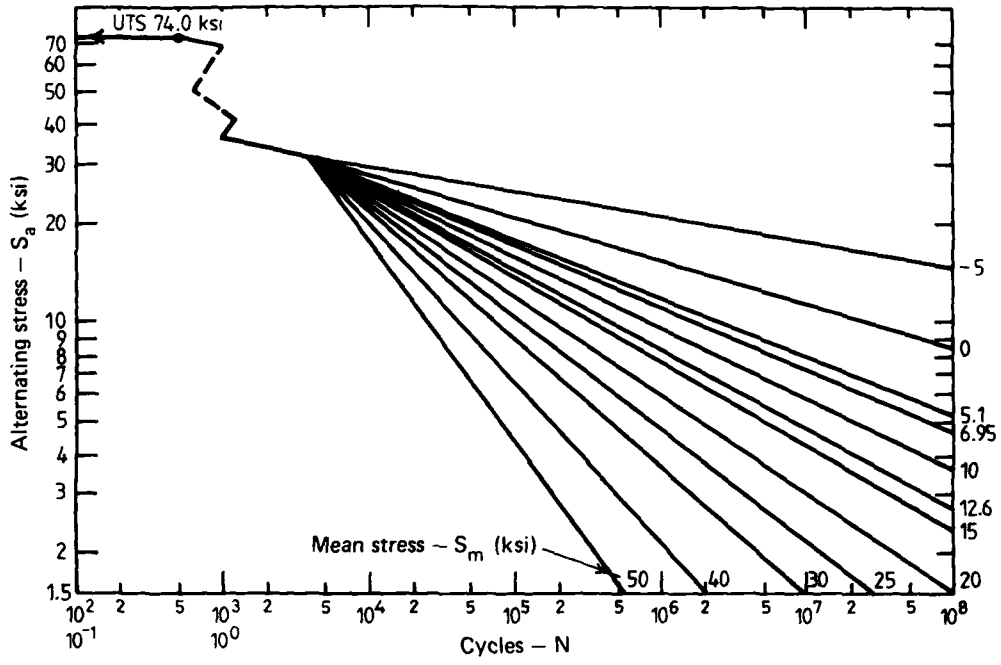

FIG. 24 FAMILY OF S/N CURVES FOR BUSHED DIMPLED-HOLE SPECIMENS

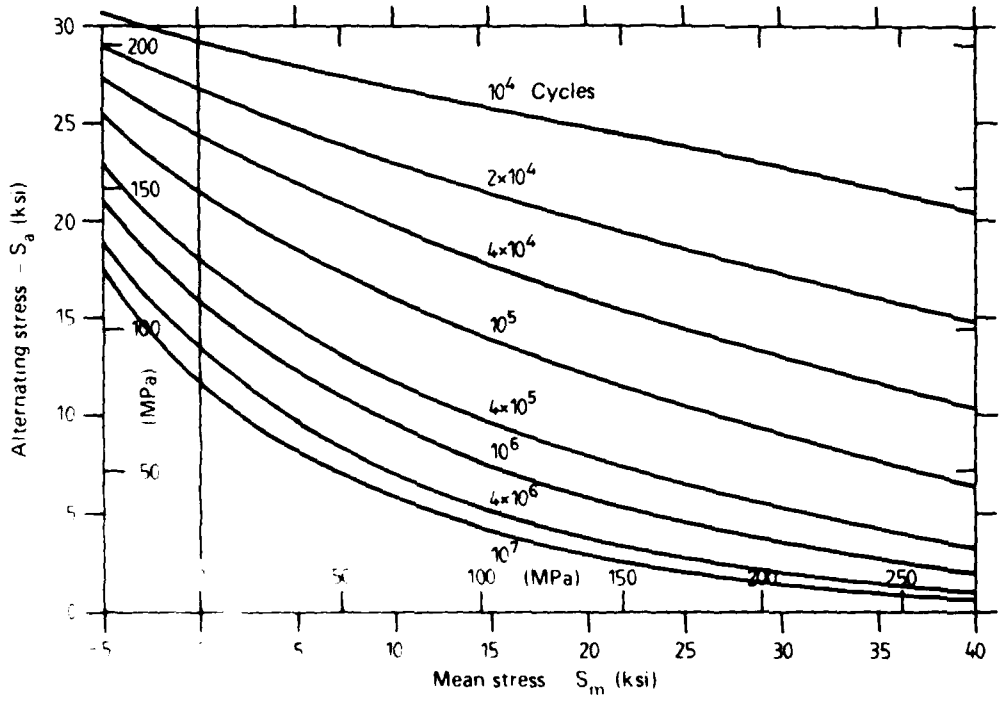

FIG. 25 S_a/S_m DIAGRAM FOR BUSHED DIMPLED HOLE SPECIMENS

DISTRIBUTION

AUSTRALIA

DEPARTMENT OF DEFENCE

Central Office

Chief Defence Scientist
Deputy Chief Defence Scientist
Superintendent, Science and Program Administration
Controller, External Relations, Projects and Analytical Studies
(1 copy)
Defence Science Adviser (UK) (Doc. Data sheet only)
Counsellor, Defence Science (USA) (Doc. Data sheet only)
Defence Central Library
Document Exchange Centre, DISB (18 copies)
Joint Intelligence Organisation
Librarian H Block, Victoria Barracks, Melbourne

Aeronautical Research Laboratories

Director
Library
Superintendent Materials
Divisional File—Structures
Authors: J. Y. Mann
G. W. Revill
R. A. Pell
G. S. Jost
J. M. Finney
C. K. Rider
J. M. Grandage

Materials Research Laboratories

Director/Library

Defence Research Centre

Library

Navy Office

Navy Scientific Adviser
Directorate of Naval Aircraft Engineering

Army Office

Scientific Adviser - Army
Engineering Development Establishment, Library

Air Force Office

Air Force Scientific Adviser
Technical Division Library
Director General Aircraft Engineering - Air Force
HQ Support Command (SMAINTSO)

HQ Support Command (SLENGO)
Australian Air Attache, Paris

Government Aircraft Factories
Manager
Library

DEPARTMENT OF AVIATION
Library
Flight Standards Division

STATUTORY AND STATE AUTHORITIES AND INDUSTRY
Trans-Australia Airlines, Library
Qantas Airways Limited
Ansett Airlines of Australia, Library
BHP, Melbourne Research Laboratories
Commonwealth Aircraft Corporation, Library
Hawker de Havilland Aust. Pty. Ltd., Bankstown, Library

UNIVERSITIES AND COLLEGES

Adelaide	Barr Smith Library
Flinders	Library
LaTrobe	Library
Melbourne	Engineering Library
Monash	Hargrave Library
	Professor I. J. Polmear, Materials Engineering
Newcastle	Library
New England	Library
Sydney	Engineering Library
NSW	Physical Sciences Library
Queensland	Library
Tasmania	Engineering Library
Western Australia	Library
RMIT	Library

CANADA
CAARC Coordinator Structures
International Civil Aviation Organization, Library
NRC
Aeronautical & Mechanical Engineering Library
Division of Mechanical Engineering, Director

Universities and Colleges

Toronto	Institute for Aerospace Studies

CZECHOSLOVAKIA
Aeronautical Research and Test Institute (Prague), Head

FRANCE
ONERA, Library
AMD-BA

M. M. Peyrony
M. D. Chaumette

INDIA
CAARC Coordinator Materials
Defence Ministry, Aero Development Establishment, Library
Hindustan Aeronautics Ltd., Library
National Aeronautical Laboratory, Information Centre

INTERNATIONAL COMMITTEE ON AERONAUTICAL FATIGUE
Per Australian ICAF Representative (25 copies)

ISRAEL
C-in-C Israel Air Force
Israel Aircraft Industries
Technion-Israel Institute of Technology
Professor J. Singer
Dr A. Buch

JAPAN
National Research Institute for Metals, Fatigue Testing Division
Institute of Space and Astronautical Science, Library

NETHERLANDS
Technical University of Delft
Professor J. Schijve
National Aerospace Laboratory (NLR), Library

NEW ZEALAND
Defence Scientific Establishment, Library
RNZAF, Vice Consul (Defence Liaison)
Transport Ministry, Airworthiness Branch, Library

Universities
Canterbury Library

SWEDEN
Aeronautical Research Institute, Library
Swedish National Defence Research Institute (FOA)

SWITZERLAND
Armament Technology and Procurement Group
F + W (Swiss Federal Aircraft Factory)
Mr L. Girard
Dr H. Boesch
Mr A. Jordi

UNITED KINGDOM

Ministry of Defence, Research, Materials and Collaboration
CAARC, Secretary
Royal Aircraft Establishment
  Bedford, Library
  Farnborough, Library
Commonwealth Air Transport Council Secretariat
National Physical Laboratory, Library
National Engineering Laboratory, Library
British Library, Lending Division
CAARC Co-ordinator, Structures
Aircraft Research Association, Library
Rolls-Royce Ltd., Aero Division Bristol, Library
Welding Institute, Library
British Aerospace
  Kingston-upon-Thames, Library
  Hatfield-Chester Division, Library
British Hovercraft Corporation Ltd., Library
Short Brothers Ltd., Technical Library

Universities and Colleges

Southampton	Library
Cranfield Institute of Technology	Library
Imperial College	Aeronautics Library

UNITED STATES OF AMERICA

NASA Scientific and Technical Information Facility
Applied Mechanics Reviews
Metals Information
The John Crerar Library
The Chemical Abstracts Service
Lockheed-California Company
Lockheed Georgia
McDonnell Aircraft Company, Library
Metals Abstracts, Editor

Universities and Colleges

Iowa	Professor R. I. Stephens
Massachusetts Inst. of Tech.	MIT Libraries

SPARES (15 copies)

TOTAL (170 copies)

This page is to be used to record information which is required by the Establishment for its own use but which will not be added to the DISTIS data base unless specifically requested.

16. Abstract (Contd)

types of specimens were between about 3 and 4·2. This compares with a ratio of 4·6 obtained for the respective full-wing scale wing fatigue tests.

For the blind anchor-nut hole specimens the predicted fatigue lives were less than those obtained experimentally at high stress scaling factors, but at low stress scaling factors the converse was the case. The ratios of the predicted lives to failure (~~Australian~~/Swiss) were much greater than those found experimentally.

Under both ~~the Australian and Swiss~~ stress spectra, the lives of front-flange bolt hole specimens incorporating interference-fit bolts were between 3 and 4 times greater than those with clearance-fit bolts.

17. Imprint

Aeronautical Research Laboratories, Melbourne

18. Document Series and Number	19. Cost Code	20. Type of Report and Period Covered
Structures Report 415	251020	

21. Computer Programs Used

22. Establishment File Ref(s)

B2/03/78, B2/03/88

Department of Defence

DOCUMENT CONTROL DATA

1. a. AR No.	1. b. Establishment No.	2. Document Date	3. Task No.
AR-003-998	ARL-STRUC-R-415	February 1985	DST 79/130

4. Title	5. Security	6. No. Pages
FATIGUE LIVES OF SPECIMENS REPRESENTING CRITICAL LOCATIONS IN MIRAGE III SPARS UNDER AUSTRALIAN AND SWISS TEST SPECTRA	a. document: Unclassified b. title: U. c. abstract: U.	28 7. No. Refs: 22

8. Author(s)	9. Downgrading Instructions
J. Y. Mann and G. W. Revill	—

10. Corporate Author and Address	11. Authority (*as appropriate*)
Aeronautical Research Laboratories, P.O. Box 4331, Melbourne, Victoria, 3001	a. Sponsor c. Downgrading b. Security d. Approval

12. Secondary Distribution (*of this document*)

Approved for public release

Overseas enquirers outside stated limitations should be referred through ASDIS, Defence Information Services Branch, Department of Defence, Campbell Park, CANBERRA, ACT, 2601.

13. a. This document may be ANNOUNCED in catalogues and awareness services available to . . .

No limitations

13. b. Citation for other purposes (*i.e. casual announcement*) may be (*select*) unrestricted (*or*) as for 13 a.

14. Descriptors		15. COSATI Group
Fatigue (materials)	Interference-fit fasteners	11130
Aluminium alloys	Load spectra	01030
Aircraft structures	Stress concentration	
Mirage aircraft	Crack propagation	
Bolted joints	Fatigue life estimation	

16. Abstract

Full-scale flight-by-flight fatigue tests on Mirage III fighter aircraft wings carried out at the Australian Aeronautical Research Laboratories (ARL) and the Swiss Eidgenössisches Flugzeugwerk (F+W) indicated much greater differences in the flights to failure than were expected. This problem has been investigated by conducting fatigue tests on specimens representing the major failure locations in the test wings — a blind anchor-nut hole ~~in the Australian case~~ and an interference-fit bolt hole ~~in the Swiss case~~ — under flight-by-flight loading sequences corresponding to those used in the full-scale tests. Constant-amplitude fatigue tests were also carried out on the blind-hole specimens to provide information for life estimation purposes, and fractographic crack propagation studies were conducted on selected blind-hole specimens.

The experimentally determined lives of both types of specimen were greater under the ~~Australian than the Swiss~~ stress spectrum. Depending on the stress scaling factor considered the life ratio ~~(Australian/Swiss flights)~~ obtained by grouping together the two stress spectra and the two

END

DATE
FILMED

1-86

DTIC